

Received February 25, 2022, accepted March 14, 2022, date of publication March 21, 2022, date of current version March 25, 2022.

Digital Object Identifier 10.1109/ACCESS.2022.3160825

# Analysis on Bending Performance of the Electro-Textile Antennas With Bandwidth Enhancement for Wearable Tracking Application

NORSYAHIRAH IZZATI ZAIDI<sup>1</sup>, NURUL HUDA ABD RAHMAN<sup>1</sup>, (Member, IEEE),  
MOHAMAD FAIZUL YAHYA<sup>2</sup>, MUHAMMAD SHAKIR AMIN NORDIN<sup>1</sup>, SUHAILA SUBAHIR<sup>1</sup>,  
YOSHIIHIDE YAMADA<sup>3,4</sup>, AND ABHIJIT MAJUMDAR<sup>5</sup>

<sup>1</sup>Antenna Research Centre, School of Electrical Engineering, College of Engineering, Universiti Teknologi MARA, Shah Alam, Selangor 40450, Malaysia

<sup>2</sup>Textile Research Group, Faculty of Applied Sciences, Universiti Teknologi MARA, Shah Alam, Selangor 40450, Malaysia

<sup>3</sup>Malaysia-Japan International Institute of Technology (MJIT), Universiti Teknologi Malaysia, Kuala Lumpur 54100, Malaysia

<sup>4</sup>National Defense Academy, Yokosuka, Kanagawa 239-8686, Japan

<sup>5</sup>Department of Textile & Fibre Engineering, Indian Institute of Technology, Delhi 110016, India

Corresponding author: Nurul Huda Abd Rahman (nurulhuda0340@uitm.edu.my)

This work was supported by the Universiti Teknologi MARA through the Young Talent Researcher Grant Scheme under Grant 600-RMC/YTR/5/3 (012/2020).

**ABSTRACT** Frequency detuning issues in antenna operation due to structural deformation have become a concern, especially for flexible devices such as a textile antenna. Under deformed conditions such as during bending, the antenna might not operate at the desired frequency, causing performance degradation. Therefore, a 1.575 GHz textile antenna for GPS tracking application with defected ground structure is proposed in this paper to alleviate the frequency detuning issues and is demonstrated under two bending conditions, H-plane and E-plane. The implementation of DGS is expected to minimize the frequency detuning by increasing the bandwidth. Hence, the frequency detuning effects could be minimized under bent conditions with broader bandwidth and acceptable antenna performance. In this paper, a planar textile-based antenna with the dimension of 90mm ( $L$ )  $\times$  100mm ( $W$ ) was designed, and three rectangular slots were applied at the ground to create DGS. A self-developed electro-textile and polyester were used as the antenna conductive material and substrate. Through the study, a detailed analysis was conducted for both antennas, with and without DGS. The significance of DGS in the proposed design is evaluated and clarified by comparing electric and magnetic field intensities in non-radiating and radiating edges. The detailed performance comparison were observed and analyzed through S-parameter, gain, radiation pattern, and current distribution. The technical performance of the proposed technique is validated through simulation and measurement. DGS implementation has improved the antenna bandwidth from 4.04% to 12.20%, with 1.45dB gain and 23.75% radiation efficiency. As a result, the antenna can operate at the desired frequency under both bending conditions. DGS method provides simplicity in its design, and this method has been widely used in conventional antennas previously. However, the detailed behaviour of field intensity around the non-radiating and radiating edges have not been demonstrated and analyzed. Therefore, the validation of the proposed design through a detailed analysis of E-field and H field intensity concerning antenna configurations; with and without DGS becomes the main contribution of this paper. In addition, the study of bending on different bending radius is also conducted in this paper.

**INDEX TERMS** Textile antenna, wearable antenna, bending, defected ground structure (DGS).

## I. INTRODUCTION

In wearable technology, smart clothing shows great potential in enhancing life value by improving clothing functionality

The associate editor coordinating the review of this manuscript and approving it for publication was Derek Abbott<sup>1</sup>.

through a combination of fabrics and electronics. The revolution of smart garments enables the wearer to experience wireless on-body communication for many applications, including wireless medical, health care, mobile communication [1], entertainment, sports, navigation [2], and tracking through global positioning system (GPS) [3], and for some

specialized occupations such as firefighters and military personnel [4]–[7].

An antenna is crucial for wearable devices as a radio wave transmitting and receiving medium to support many wireless communication aspects such as in-body communication, on-body communication, and off-body communication [8]. The wearable antenna must be lightweight, flexible, and easily embedded in the garment [9]. Thus, for this emerging technology, the conventional antenna type is no longer relevant to wearable applications due to its rigid and non-flexible characteristics. Therefore, the use of a more flexible material, such as fabric-based material, is encouraged.

The conventional textile-based wearable antenna is usually fabricated using a regular fabric and then integrated with a radiating element such as copper foil, copper tape, copper powder, conductive spray, or adhesive sheets such as ShieldIt™ and Zelt® [10], [11]. Integrating these radiating elements into the antenna is usually done through gluing, spraying, and ironing. These methods provide an easy fabrication of the textile antenna; however, there is also a drawback, specifically on sustainability issues. The antenna can be easily detached from the fabric after being worn or washed several times [12], which will cause a reduction in antenna efficiency and influence the antenna performance due to the dissolution of conductive material from the textile. Therefore, a more durable conductive textile that is more structurally practical and comfortable was developed in this study, as shown in Figure 1.

The movement of a human body consists of a superposition of bends in arbitrary directions. In textile antennas, mechanical deformation such as bending is unavoidable. It is known that the effect of bending will degrade the antenna performance, such as its gain, bandwidth and may shift its resonant frequency for the intended application [13]–[15] due to the change in impedance characteristic when bending occur [16]. In a worst-case scenario (significant E-plane bent condition), the frequency can be drifted from the intended application due to the input matching that is no longer effective (mismatch). Thus, the  $S_{11}$  will be less than  $-10$  dB at the application frequency [17]. Due to this scenario, the antenna

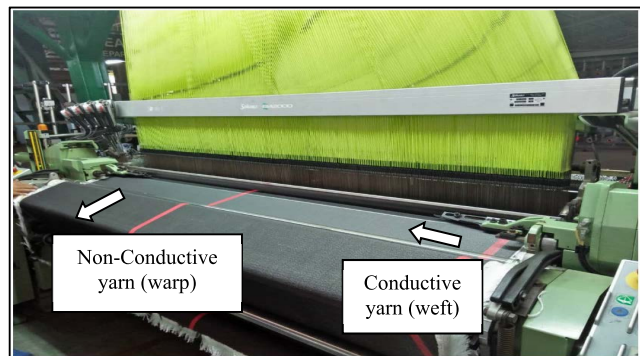


**FIGURE 1.** Warp and weft of the manufactured conductive textile. The conductive yarn is a mixture of copper and polyester, and the non-conductive yarn is polyester.

might not work and radiate for the designated application. Thus, a wideband operation is suggested to alleviate these effects and maintain the antenna performance under bending to ensure that the resonant frequency remains within the operating region even after bending [18].

Previously, an ultra-wideband antenna has been used to minimize the frequency detuning during bending; however, the analysis is limited to the H-plane bent condition [19]. Similarly, in [20]–[22], the bending effects under various bending radius and angles were presented, yet the antenna performance on E-plane bent was not discussed. A study on the wideband antenna concerning H-plane and E-plane bent conditions was performed by [23]. Nevertheless, the material used was not textile-based; thus, the accuracy shall be validated further. As in [24], simulation and analysis on H- and E-plane bent conditions were performed, but the data was not validated with the measured data. The most related work was shown in [25]. The observation on the UWB textile antenna in H-plane and E-plane bent condition is performed, and the simulation analysis was verified with the measured data. However, a detailed analysis of the antenna gain, radiation pattern, and current distribution on both H-plane and E-plane bent conditions was not shown.

This paper proposes wider bandwidth to mitigate the frequency detuning issue in the GPS textile-based wearable antenna. Many techniques have been used to enhance antenna bandwidth in wearable applications, such as slots and slits in [26] and modified octagonal patches [27]. However, this technique is not suitable or practical to this project due to the high possibility of the yarn being detached from the fabric during fabrication, especially for the self-developed conductive textile, which may contribute to the antenna performance degradation. Shorting pin technique by [28] is also identified to increase the bandwidth of the textile antenna. Yet, its practicality is still an issue due to the complexity of the shorting pin for a flexible structure. Similarly, in [29], the bandwidth was improved using a stacked technique, and multiple bands were achieved. However, the combination of jeans fabric and foam as the antenna substrate is not practical in wearable applications. Several bandwidth enhancement techniques have been presented in [30] and [31]. In the papers, multiple design methods are implemented on a single antenna, such as stub, AMC, metallic walls, printed strip, shorting walls, and air gap, making it complex and thick in structure. Therefore, the proposed technique is not suitable for textile antenna materials. Based on the analysis in [32]–[34], the bandwidth could also be improved by using Defected Ground Structure method (DGS). This method is one of the most suitable methods for the proposed design since the etched slots or defects are done on the ground.

Therefore, in this paper, a planar antenna with bandwidth enhancement using defected ground structure (DGS) was designed to solve the frequency detuning problem. The analysis was conducted by studying the antenna characteristics due to bending, including gain, resonant frequency, and radiation pattern on H-plane and E-plane bent conditions. A cylindrical

foam with a radius of 42.5 mm and bending angle of approximately 135°, was used, representing the bending condition around the human arm. A self-developed conductive textile and polyester fabric was used as a radiating element and substrate of the antenna with the dielectric constant,  $\epsilon_r$  of  $1.05 \times 10^4$  and 1.36 respectively. Here, the study was on bending conditions only without considering the dielectric loading effects due to the human body. The antenna was designed at 1.575 GHz frequency for GPS application. All the simulation works were done using 3D electromagnetic software, known as CST, and the validation of results was done through laboratory measurement. The achieved S-parameters (at different bending angles), the currents and fields distributions of both the radiating elements and the ground plane with different slots are all numerically and experimentally measured in the field of free space. Figure 2 shows the example of GPS tracking system that can be used to trace a child location.

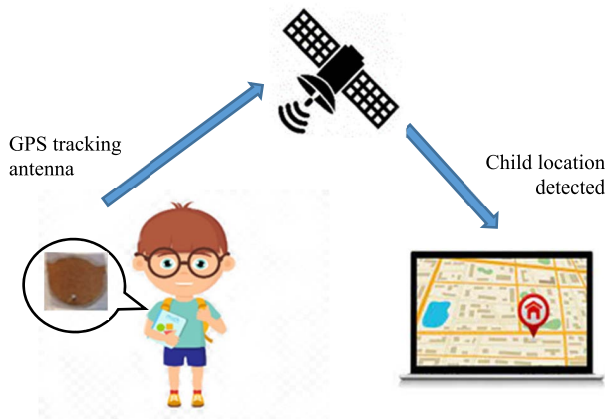


FIGURE 2. Example of a GPS tracking system using wearable textile antenna integrated with children school attire.

## II. METHODOLOGY

This section describes the methodology related to the development of conductive textile and antenna design.

### A. DEVELOPMENT OF CONDUCTIVE TEXTILE

The development of conductive textile started with the production of conductive yarn, also called hybrid yarn, a combination of copper and polyester yarn. By using the hollow spindle spinning method, copper-covered yarn was produced [35]. The copper yarn of 0.14mm diameter was twisted around the polyester yarn during the production, as shown in Figure 3. Based on the previous study in [36], [37], copper covered-yarn design structure is chosen because it contains a higher ratio of copper-to-polyester thread than copper core-sheathed yarn, which contributes to the higher value of textile conductivity. This hybrid yarn alignment is better than the conventional copper core-sheathed yarn, where the copper yarn is kept as the core and is wrapped around with the polyester yarn.

After that, the process continued with the production of conductive textile using SULZER TEXTILE G6300 rapier

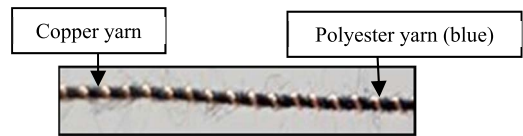


FIGURE 3. Copper covered yarn.

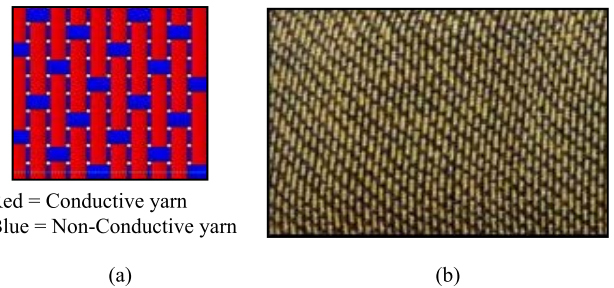


FIGURE 4. (a) Satin weaving structure (b) Satin conductive textile.

TABLE 1. The physical and electrical properties of conductive textile.

Properties	Values
Conductivity ( $\sigma$ )	$9.26 \times 10^4$ S/m
Thickness (t)	0.36 mm
Textile composition	83% Copper + 17% Polyester

weaving machine, as shown previously in Figure 1. The satin weaving technique was chosen as it provides better antenna gain performance due to its interweaving ratio arrangement, as reported in [38]. The conductive yarns were interlaced with non-conductive yarns to make the textile comfy and suitable to be worn. The conductivity of the conductive textile was measured using a stripline measurement technique [39]. Figure 4 and Table 1 show the woven conductive textile and its electrical properties, respectively.

### B. ANTENNA DESIGN

A circular-shaped planar textile antenna was chosen in this paper to provide a more stable gain and less frequency detuning effect during bending as compared to a square and edgy flower patch shape [40]. The feeding technique used was coaxial feed to minimize the fabrication error that may happen during antenna fabrication contributing to the impedance mismatch and other performance degradation [41]. Three rectangular slots were designed on the ground plane to increase the antenna bandwidth. A simple rectangular shape design is proposed to simplify the analysis as a rectangular shape is symmetrical. The location of slots was chosen based on the location of feed, where it shall be at the same plane beside the transmission line in the co-planar waveguide [42] or under the transmission line [43]. It is because the current flow is the strongest around the feed. Following the quasi-static principle of DGS [44], the quasi-transverse electromagnetic mode (TEM) propagates under the microstrip filament (where the current and electromagnetic field is confined)

and the infinite ground plane in a conventional microstrip transmission line. The return current on the ground plane represents the negative image of the current distribution on the microstrip line. In the presence of DGS, the current return path is disturbed as the current is confined to the periphery of the perturbation. It will return to the underneath of the microstrip line once the perturbation is over [45]. The disturbance of current distribution on the ground plane may change the characteristics of a transmission line (or any structure) by including some parameters such as slot resistance, slot capacitance, and slot inductance to the line parameters (line resistance, line capacitance, and line inductance) [46]. Therefore, the changes in the current distribution due to DGS will be demonstrated in the next section.

The geometry of the proposed antenna design, without and with DGS, labeled in this manuscript as Antenna 1 and Antenna 2, respectively, is shown in Figure 5. Table 2 shows the antenna dimensions. To demonstrate the ability of the proposed design to mitigate the frequency detuning issues, bending condition along E-plane and H-plane was shown through simulation and measurement as shown in Figure 6 and 7, respectively.

**C. PARAMETRIC ANALYSIS OF ANTENNA DESIGN**

A parametric analysis is performed to investigate the characteristics of the proposed antenna when the antenna’s ground structure is modified through the implementation of defected ground structure (DGS). The modification of the ground layer is done to increase the bandwidth in order to minimize the detuning effects. Theoretically, the metallic part of the microstrip antenna is the combination of resistance, inductance, and capacitance. So, when DGS is integrated on

**TABLE 2. Parameters and dimensions of the fabricated antenna.**

Parameters	Dimensions (mm)
a	90
b	100
c	90
d	15
e	45
f	3
g	18
r	38

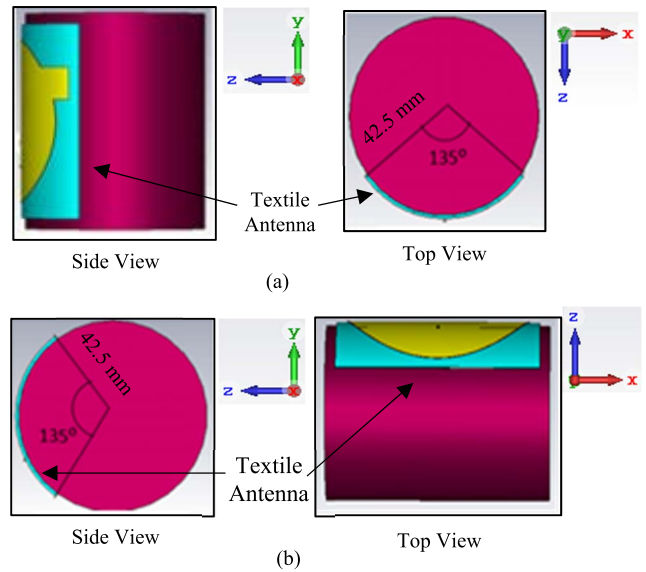


**FIGURE 6. Side view and top view of bending condition (a) H-plane (b) E-plane.**

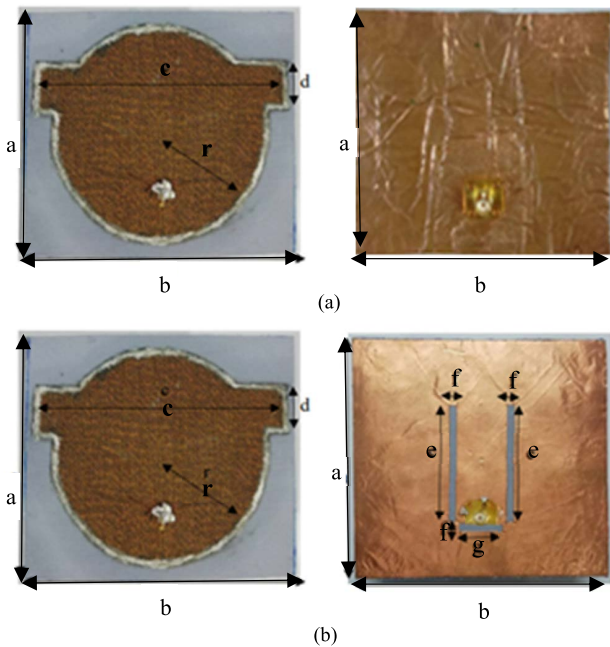


**FIGURE 5. Geometry of the fabricated antenna design (a) without DGS (Antenna 1) (b) with DGS (Antenna 2).**

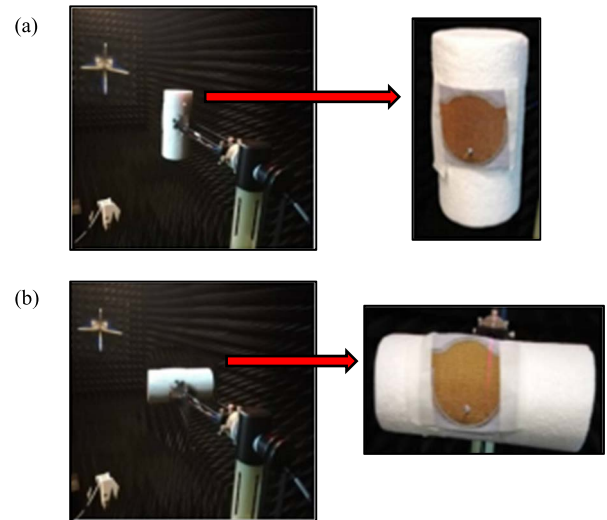


**FIGURE 7. Measurement of antenna under bending conditions (a) H-plane (b) E-plane.**

the ground plane under the transmission line, the defected region will disturb the ground plane’s current distribution. In other words, by adding slots on the ground plane, the transmission line characteristics, specifically the effective capacitance, inductance, and resistance values will change.

This working principle is employed in the antenna design as it is known to increase the antenna bandwidth [47]–[49]. The parametric analysis in this section is done to identify the most optimum DGS structure that will solve the frequency detuning problems. The study parameters are the slot’s locations, the number of slots, the slot’s thickness, and the slot length and width.

1) SLOT LOCATIONS

The slots at the ground plane are placed underneath the patch concerning the coaxial probe position. The current is significantly higher at the coaxial probe point to intentionally disturb the shielded current distribution on the ground plane. As a result, the excitation and propagation of the electromagnetic wave through the substrate layer can be controlled [50]. The location of the slot is as shown in Figure 8. The effects of the slot position on the coaxial probe location at the ground plane are studied in the  $S_{11}$  graph and current distribution as shown in Figures 9 and 10.

Based on Figure 9, when a slot is placed vertically on the left and the right side of the coaxial probe, it has resulted in the same pattern with a slight reduction in  $S_{11}$  and the same resonant frequency. However, when the slot is placed horizontally above and below the coaxial probe, the  $S_{11}$  is degraded by almost half as compared to the original (without a slot). The resonant frequency is also shifted, and the shifting is more significant when the slot is placed above the coaxial probe. Meanwhile, Figure 9 shows that even though the current distribution on the ground plane is disturbed, the bandwidth remains the same when only one slot is applied. Implementing one slot is not sufficient to disturb the current distribution on the ground plane and change the bandwidth. The changes only show a slight shift in resonant frequency and degradation in  $S_{11}$ . Hence, the investigation was continued with the implementation of more slots

2) NUMBER OF SLOTS

In this experiment, the number of slots is increased to improve the antenna bandwidth. The conducted study is as shown in Figure 11.

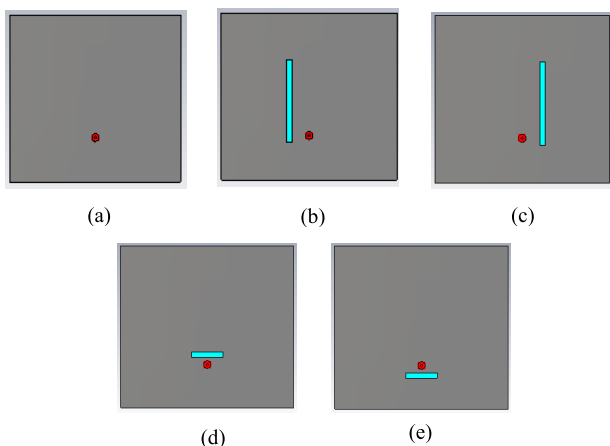


FIGURE 8. Slot locations (a) No slot (b) Left slot (c) Right slot (d) Upper slot (e) Lower slot.

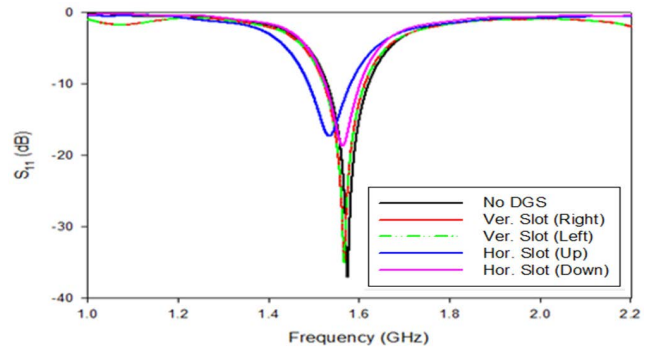


FIGURE 9. Effects of slot locations on the ground plane to the  $S_{11}$  performance.

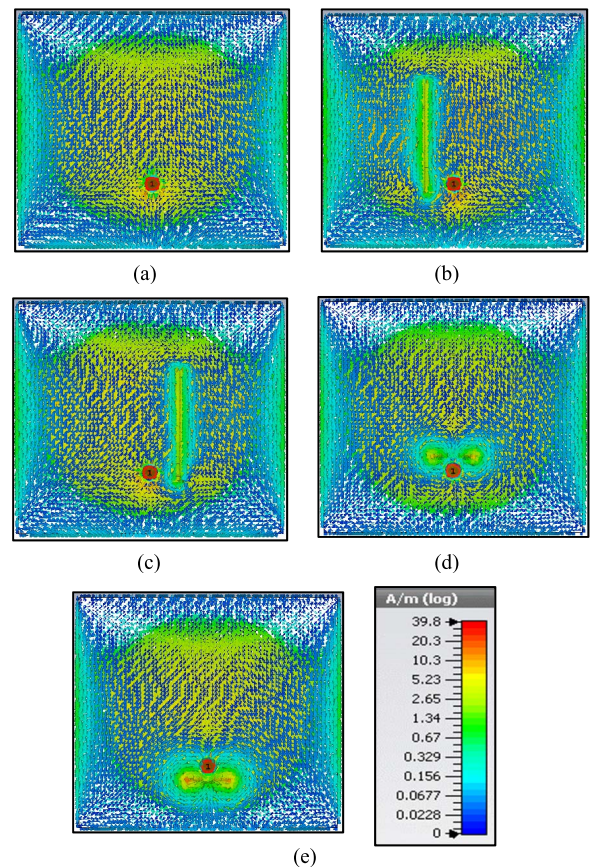
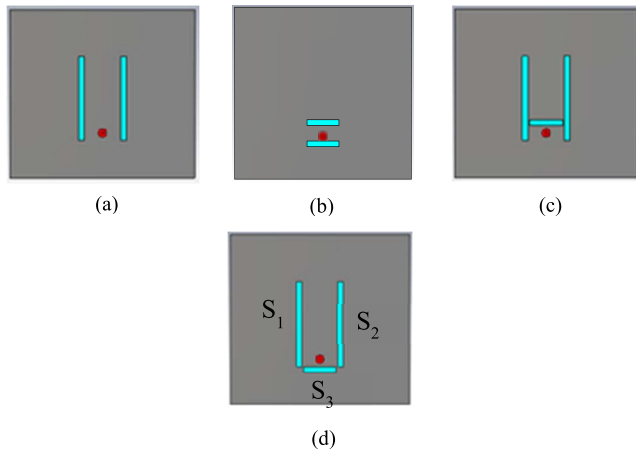


FIGURE 10. Current distribution at the ground plane concerning the slot locations (a) No slot (b) Left slot (c) Right slot (d) Upper slot (e) Lower slot.

Figure 12 shows that the bandwidth is increased when two slots are placed vertically between the coaxial probe. By referring to the current distribution in Figure 13(a), it can be observed that the addition of slots has created another disturbance in the current flow, hence, creating another  $S_{11}$  operational band and increasing the bandwidth. However, the antenna is less efficient since the  $S_{11}$  is above  $-10$  dB. Then, another trial is done using two slots placed horizontally between the coaxial probe. The result indicates no changes to the bandwidth as the bandwidth remains narrow. This is



**FIGURE 11.** Number of slots on the antenna (a) Double slot (vertical) (b) Double slot (horizontal) (c) Double slot (vertical) with third slot above the port (d) Double slot (vertical) with third slot below the port.

because, as seen in Figure 13(b), the current flow shows that the disturbance in the surface that happened in both slots seems to combine and form one circular current. The current concentration of two slots became one in the horizontal position; hence the results are more significant than the one slot results. The outcome of the two vertical slots is more promising as the bandwidth widens. Thus the third slot is applied to the ground plane for better bandwidth performance.

The addition of a third horizontal slot produces three current circulations on the ground plane, as shown in Figure 13(c) and (d), and increases the bandwidth. However, the antenna operates in dual-band mode and the frequency is shifted to the left. Next, the third slot is located to be under the coaxial probe. This modification resulted in wide bandwidth with  $S_{11}$  values of below  $-10$  dB. Hence, the requirement is satisfied.

Typically, the slots can be represented by purely reactive impedance and a network of impedance, which can also be designed to give a broadband response and increase the antenna bandwidth [51]. When DGS is applied on the ground plane, the fringing field increases; thus parasitic capacitance is introduced. Due to parasitic capacitance, the coupling between the conducting patch and the ground plane increased, which enhanced the bandwidth. Whenever any slot is cut on the ground, the longitudinal current flow is interrupted, and the direction of the current is changed, causing an increase in bandwidth [52]–[54].

### 3) DISTANCE OF SLOTS

In this investigation, the distance of slots is studied to obtain wider bandwidth results. The experiment begin by varying the distance of vertical slot,  $d_v$  first, and then the horizontal slot,  $d_h$  as shown in Figure 14. Coaxial feed was indicated as the reference point to the position of slots. Figure 15 represents the  $S_{11}$  by varying the  $d_v$  with respect to the coaxial probe, while Figure 16 shows the results of varying the  $d_h$ . The current distribution is shown in Figure 17 and 18 accordingly.

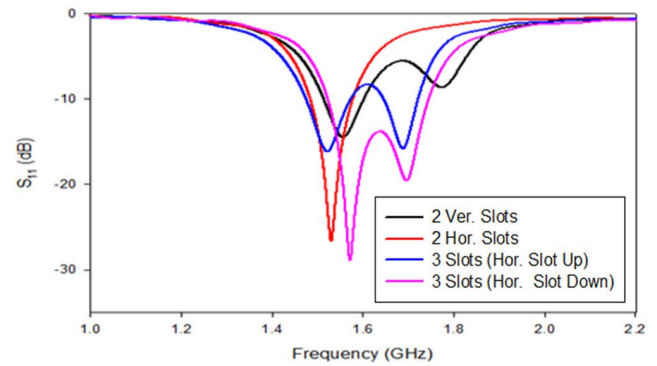


**FIGURE 12.** Effects of number of slots to the antenna bandwidth.

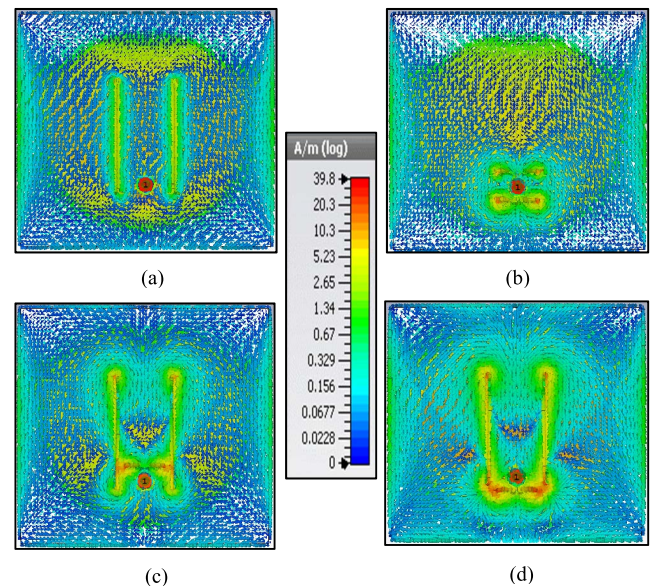


**FIGURE 13.** Current distribution at the ground plane concerning the number of slots (a) Double slot (vertical) (b) Double slot (horizontal) (c) Double slot (vertical) with third slot above the port (d) Double slot (vertical) with third slot below the port.

Through this experiment, the sizes of horizontal and vertical slots have been unchanged.

As observed in Figure 15, the distance of 4mm to 8mm shows a narrow bandwidth. Due to the small distance between both slots, the current intensities are added up. The current is circulated at the center of the antenna and forms a single current disturbance (as shown in Figure 16(a), (b) and (c)). It is also observed that as the distance of slots increases (from 4mm to 10 mm), the resonant frequency shifts to the right. The increment in distance or gaps has increased the effective inductance; hence the frequency is shifted to the higher frequency [55]. Changes in bandwidth are established at the slots distance of 10 mm and 12 mm. These separations provide adequate space for the current to circulate on its periphery, eventually making the current field on the slot stronger and disturbing the current distribution. Thus, the condition shown in Figure 16(d) and (e) produce wider bandwidth. However, as the slot is located too far from the coaxial feed, the current

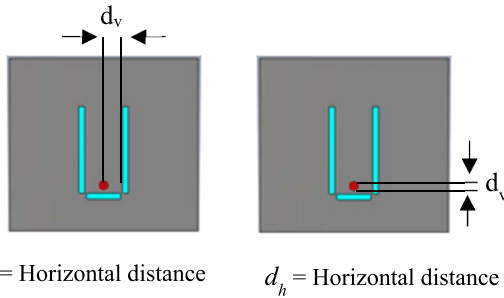


FIGURE 14. Optimization of slot position by varying the horizontal slot,  $d_h$  and vertical slot,  $d_v$ .

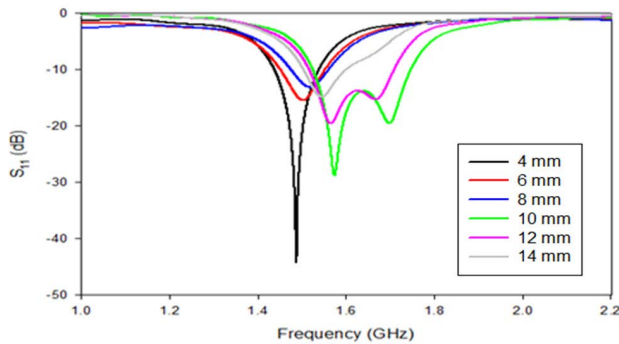


FIGURE 15.  $S_{11}$  of the optimization of slot position with respect to the distance of horizontal slot,  $d_h$ .

distribution became weaker (as in Figure 16(f), thus unable to produce wide bandwidth. Therefore based on the performance of  $S_{11}$  and current distribution, the optimum distance for vertical slots is 10 mm.

Next, the distance of the horizontal slot concerning the coaxial probe is varied, where at the same time, the vertical slots are maintained at the 10 mm distance. By varying the distance of the horizontal slot, it can be seen that the bandwidth is almost similar, but the  $S_{11}$  shows differences. Here, the analysis focuses on reducing the peak at the center of the bandwidth (as shown in Figure 17). From the graph, as the distance increases, the rising peak shown by the circle area increases and approaches  $-10$  dB. This phenomenon is related to the current distribution on the ground plane (as shown in Figure 18). The current circulating the slots becomes weaker as the horizontal slot moves away from the coaxial feed. Hence the  $S_{11}$  becomes the lowest. Thus, the optimum distance of the horizontal slot is chosen to be 5 mm because the  $S_{11}$  is the better. The optimized  $d_v = 10$  mm and  $d_h = 5$  mm are used for antenna 2.

#### 4) LENGTH OF SLOTS

In this section, the analysis was based on the lengths of the vertical slots ( $L_1$  and  $L_2$ ) and the horizontal slot ( $L_3$ ) as shown in Figure 19. Figure 20 shows the optimization results of the length of the vertical slots ( $L_1$  and  $L_2$ ). The length of the slots is varied from 10 mm to 50 mm.

Figure 20(a) shows a significant observation at 30 mm and 40 mm, where the dual-band operation occurs. Meanwhile,

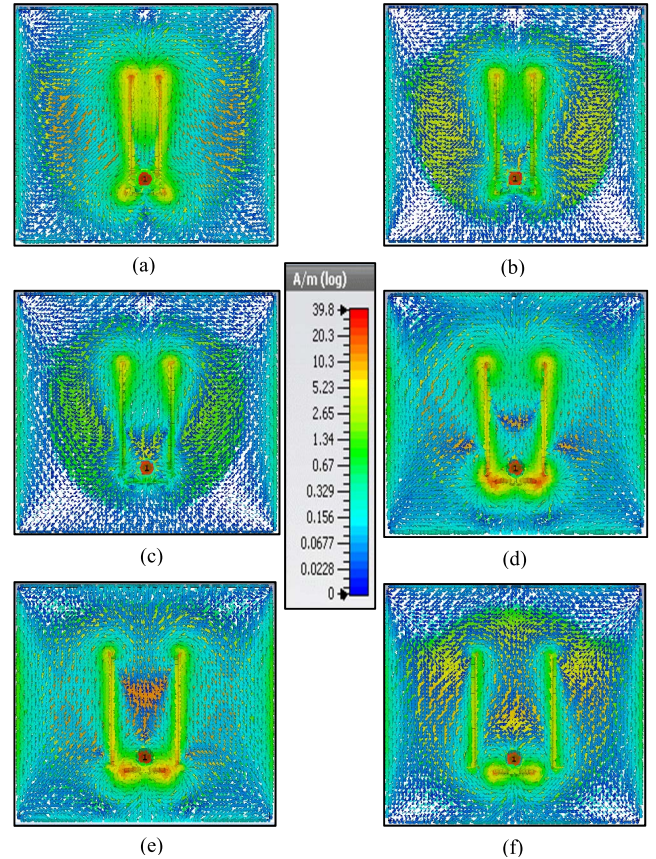


FIGURE 16. Current distribution at the ground plane with respect to the distance of horizontal slot,  $d_h$  (a) 4mm (b) 6mm (c) 8mm (d) 10mm (e) 12mm (f) 14mm.

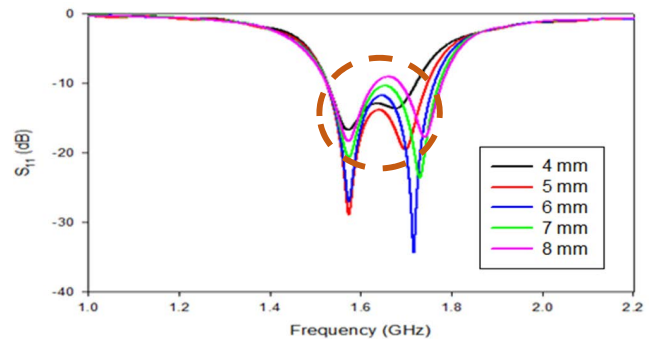
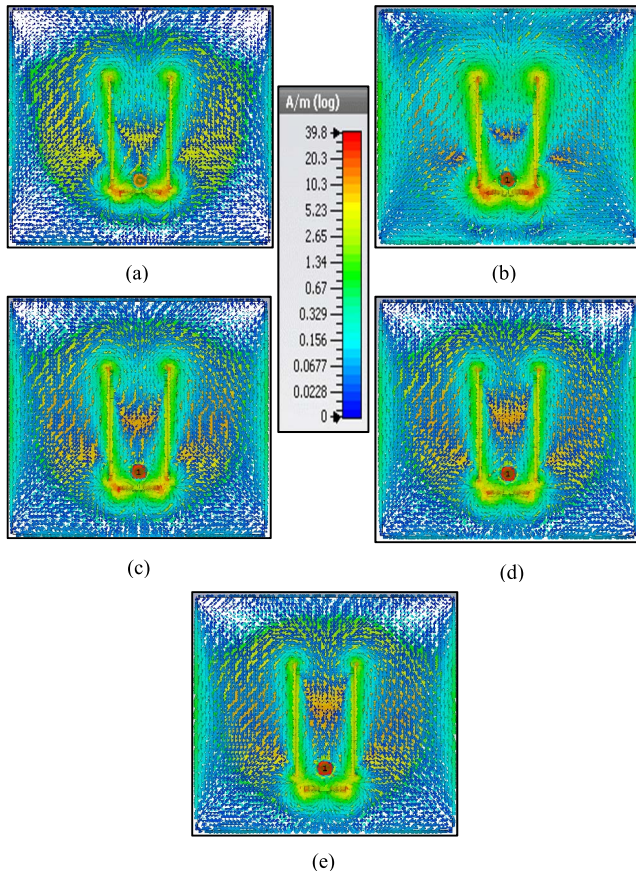
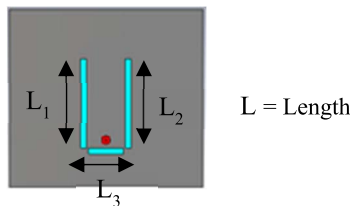


FIGURE 17.  $S_{11}$  of the optimization of slot position with respect to the distance of vertical slot,  $d_v$ .

at 50 mm, the  $S_{11}$  is narrowed. The graph shows a trend, starting from the length of 30 mm; as the size increased, the dual-band frequency became narrow, and simultaneously, the  $S_{11}$  at the rising peak between the two bands became lower. Thus, towards approaching 50 mm length, the probability of achieving a wide bandwidth is high. Therefore, the scale is narrowed to half of the length between 40 mm to 50 mm. The length of vertical slots is simulated at 45 mm and with a tolerance length of 1 mm. So three new lengths are simulated at 44 mm, 45 mm, and 46 mm, as represented in Figure 20(b). Based on Figure 20(b), the length of 44 mm is not qualified



**FIGURE 18.** Current distribution at the ground plane with respect to the distance of horizontal slot,  $d_h$  (a) 4mm (b) 5mm (c) 6mm (d) 7mm (e) 8mm.



**FIGURE 19.** Optimization of slots length.

as it shows a dual-band operation. Then, for 46 mm, a wide bandwidth is achieved, but it is not the optimum bandwidth. The highest bandwidth obtained is at the length of 45 mm. The graph also shows a trend, as the length of the slot increases, the bandwidth decreases.

Next, the length optimization is conducted for the horizontal slot,  $L_3$ . The effects of the length of the horizontal slot are studied in Figure 21. These results show a slight decrease in bandwidth as the slot length increases. However, the main changes in the  $L_3$  slot can be observed at the rising peak of the  $S_{11}$ . The  $S_{11}$  value at the peak became lower as the length increased. Two potential widths of 8 and 9 mm, are evaluated since the  $S_{11}$  at the peak is below  $-10$  dB. In this situation, both dimensions show wideband characteristics, and the difference in bandwidth is only 1%. Both lengths are then compared in terms of the  $S_{11}$  value. Based on the

evaluation, 9mm length is the optimum value of the horizontal slots. Thus, the optimum length of the vertical slots and the horizontal slot are verified.

From the analysis of slot length, the presence of slots has interrupted the current flow as shown in the current distribution diagram in Figure 16 and 17. Increasing the slot length has increased the path length of the surface current around the slot, thus is increasing the reactive loading and changing the resonant frequency [51]. An increment in reactive loading also affects the Q factor of the RLC circuit, which corresponds to the bandwidth, as shown in Equation (1) and (2). By increasing the length of the slot, the effective inductance is increased. An increase in the effective inductance causes an increase in the Q factor of the RLC circuit; hence the antenna bandwidth is decreased [56], [57]. The relation of bandwidth,  $BW$ , center frequency,  $F_c$  and Q factor,  $Q$  of the resonant circuit is shown by Equation (1), where  $Q$  is directly proportional to  $X$ , the capacitive or inductive reactant at resonance, and inversely proportional to  $R$ , the resistance as shown by the Equation (2) and (3) [58]–[60].

$$BW = \frac{F_c}{Q} \tag{1}$$

$$Q = \frac{X}{R} = \frac{X_c}{R} \text{ or } \frac{X_L}{R} \tag{2}$$

$$\frac{X_c}{R} = \frac{1}{\omega RC} \text{ or } \frac{X_L}{R} = \frac{\omega L}{R} \tag{3}$$

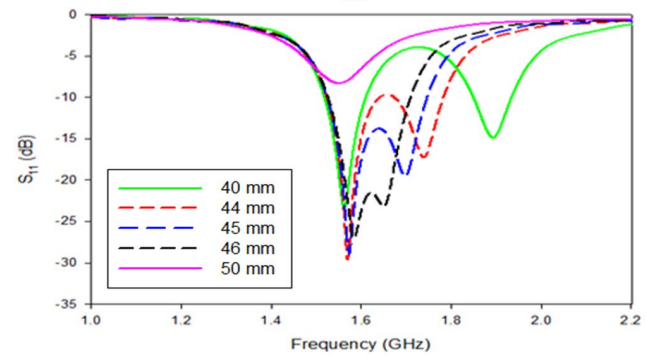
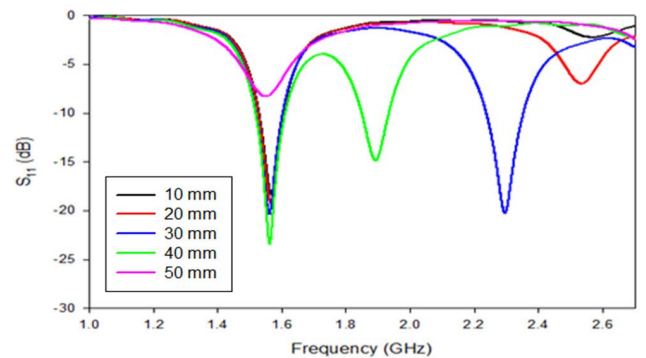


**FIGURE 20.** Optimization of vertical slots length  $L_1$  and  $L_2$  (a) with multiplier of 10 mm (b) at minimize range.



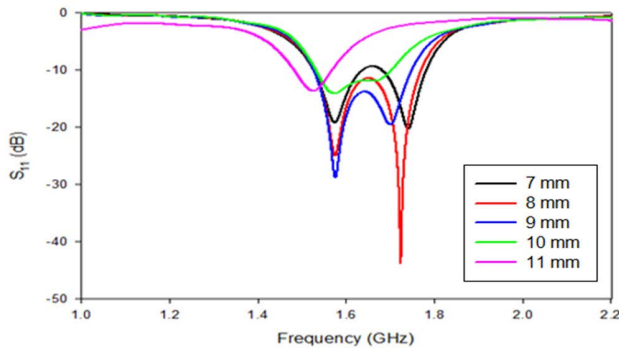


FIGURE 21. Optimization of horizontal slot length  $L_3$  at 7mm to 11mm.

5) WIDTH OF SLOTS

In Figure 22, the widths of the three slots are varied simultaneously, and the results are analyzed in Figure 23.

As the width of slots increases, the bandwidth is reduced. At the width of 3 and 4 mm, the antenna has achieved wide bandwidth. However, the optimum was 3mm because the bandwidth was larger. Even though the  $S_{11}$  for 4 mm width is high, the main objective is to get the optimum bandwidth. Hence, the width of 3 mm is the suitable width in the design. The increment in the slot width will decrease the effective capacitance. The decrease in capacitance will increase the Q factor; hence, the antenna’s bandwidth will decrease [56], [57]. The fundamental concept of width is the same as length, where optimizing the length and width of the slots will result in the optimum bandwidth. The relation between the bandwidth and the Q-factor is as shown in Equation (1), and the correlation between Q factor with capacitance,  $C$  is shown in Equation (4).

$$Q = \frac{1}{\omega RC} \tag{4}$$

III. RESULT AND DISCUSSION

This section discusses the analysis of the antenna performance in relation to  $S_{11}$  parameters, radiation performance, and current distributions under normal (flat), H-plane and E-plane bent condition.

A.  $S_{11}$  PARAMETERS

The implementation of DGS has improved the antenna bandwidth from 74 MHz to 226 MHz. From the study, as the antenna is bent, the resonant frequency shifts in both bending conditions due to the changes in the antenna’s effective length during bending [61]. It is also observed that

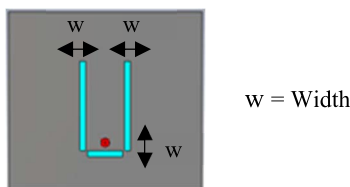


FIGURE 22. Optimization of slots width.

the resonant frequency is shifted to the left as the antenna is bent (as shown in Figure 24). These scenarios can be related to the increment in capacitive reactance and changes in load impedance caused by bending [62], [63]. The relationship between the frequency and capacitive reactance can be analyzed through the impedance versus frequency graph, as shown in Figure 25 [64].

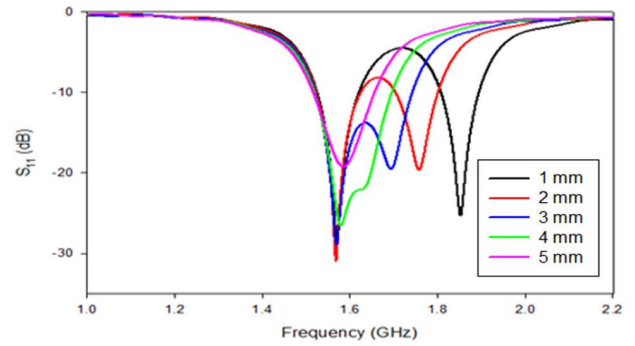


FIGURE 23. Optimization of horizontal slots width,  $w$  at 1mm to 5mm.

In theory, based on the graph in Figure 25, when there is an increment of capacitive reactance in the antenna, the new resonant frequency,  $f$ , will be shifted to the left ( $f < Fr$ ). Meanwhile, the frequency will be shifted to the right ( $f > Fr$ ) if there is an increment in inductive reactance in the antenna. In this case, the resonant frequency  $Fr$  is 1.575 GHz, and the  $f$  is shifted to the lower frequency as the antenna is bent; thus, there is an increment in capacitive reactance to the antenna. Equation (5) represents the relationship between capacitive reactant,  $X_c$ , and frequency,  $f$ , where  $X_c$  is inversely proportional to  $f$ . Therefore, adding a capacitive reactance will decrease the resonant frequency [65].

$$X_c = \frac{1}{2\pi fC} \tag{5}$$

The analysis also shows that the frequency detuning is more significant when the antenna is bent along the E-plane than H-plane. This is because when it is bent along the E-plane, the affected bent area is at the radiating plane. The effective length along the current flow is disturbed; thus, the frequency shifting is apparent on E-plane compared to H-plane. As presented in Figure 24(c), the frequency was shifted for Antenna1, but as the bandwidth becomes larger with the aid of DGS, the antenna can work at its operational frequency with an excellent  $S_{11}$  value even though there is a slight shift in the resonant frequency.

The significant discrepancy is observed in the measured E-plane bent condition due to the multiple bending effects on the antenna during the measurement. The same antenna was used for measurement on the H-plane condition; and the E-plane bent condition. Multiple uses of the same antenna for measurement might also contribute to the change in the effective length of the slot and transmission line as the antenna is bent, which eventually has detuned the input impedance of the

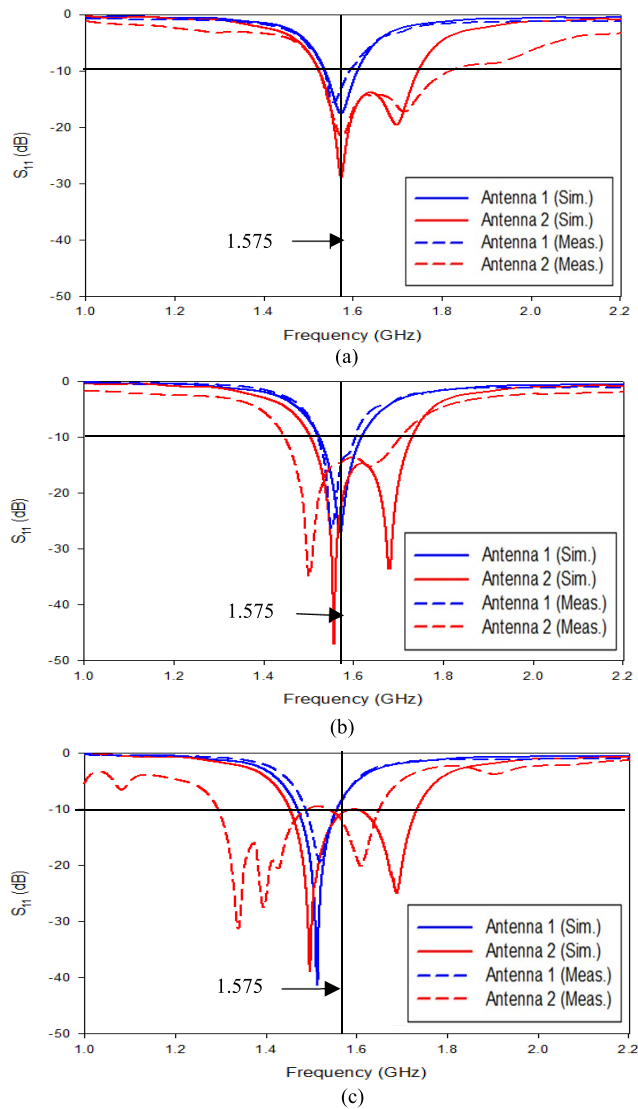


**FIGURE 24.**  $S_{11}$  parameters of simulated and measured Antenna 1 and Antenna 2 in (a) normal (b) H-plane and (c) E-plane bent conditions.

antenna [66]. Nevertheless, the antenna can still operate at the desired frequency, proving that an improvement in bandwidth has significantly solved the frequency detuning issues.

**B. RADIATION PATTERN AND GAIN**

Figure 26 and Table 3 show the radiation pattern and the gain of antenna 1 and 2, respectively. The results of gain and efficiency is also summarized in Figure 27. As observed in Table 3, the gain of the antenna is increased when it is bent on H-plane and decreased in E-plane bent condition. The effect of bending can also be observed in the antenna radiation pattern, where its relation to antenna gain is explained through the current distribution in Figure 28 and Figure 29.

Figures 26(a) and (b) show that the antenna back lobe is reduced as it is bent on H-plane. However, the back lobe becomes bigger as it is bent on E-plane. This scenario happened because when the antenna is in a flat condition, the

current is equally distributed, as shown in Figure 28(a) and Figure 29(a). As the antenna is bent on H-plane, the current direction is on the same plane as the bending. Therefore, the high current density is observed and accumulated at the center of the antenna, which eventually contributes to high magnetic fields in the antenna (Figure 28(b) and Figure 29(b)). Hence, this has increased the antenna gain and reduced the antenna back lobe.

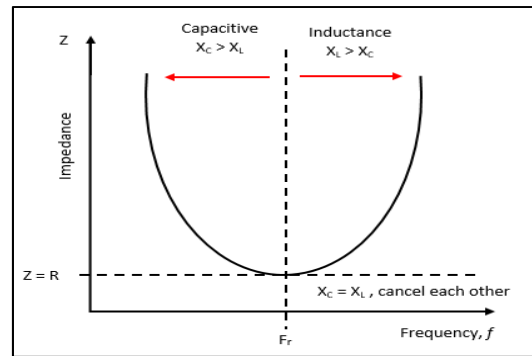


**FIGURE 25.** Graph impedance vs frequency for series RLC resonance circuit.

Meanwhile, as the antenna is bent on E-plane, the effective current length on the antenna is distorted. The surface current disperses to both sides of the antenna and yields a magnetic field on each side of the antenna (Figure 28(c) and Figure 29(c)). Therefore, this has caused the radiation of the antenna to disperse on the side, which has contributed towards the increment of the antenna back lobe and side lobe and caused gain degradation. The behaviour of the current during bending for both Antenna 1 and Antenna 2 are similar. However, the implementation of DGS on Antenna 2 has slightly degraded the antenna gain performance. This is due to the increment in the antenna back radiation [67], [68], which is observed through the radiation pattern in Figure 26(b).

From the axial ratio result shown in Figure 30, antenna 1 and 2 are linearly polarized. The simulated and measured radiation pattern for both antenna co-polarization and cross-polarization in flat and bending conditions are shown in Figure 31, 32, and 33. As observed in Figure 31, 32 and 33, the radiation patterns for antenna 1 and 2 are almost similar in co-polarization conditions. However, in a cross-polarization state, antenna 2 shows broader beam as compared to antenna 1. Since the antenna is linear polarized, in this case, it shows that the radiation of antenna 2 is wider at the non-desired polarization direction. Therefore, the gain in antenna 2 is slightly decreased as compared to antenna 1. Further explanation on the antenna E-field and H-field is discussed in the next section.

**C. E-FIELD AND H-FIELD OF THE ANTENNAS**

Figure 34 shows the electric field intensity of both designs inside the antenna layer along the non-radiating edges (y-axis). Theoretically, the graph accurately represents both conditions, where the E-field intensity is zero at the mid-patch

**TABLE 3.** Simulated and measured gain of Antenna 1 and Antenna 2 in flat, h-plane and E-plane bending conditions.

Bending Conditions	Gain (dB)				Efficiency (%)			
	Simulated Antenna		Measured Antenna		Simulated Antenna		Measured Antenna	
	Antenna 1	Antenna 2	Antenna 1	Antenna 2	Antenna 1	Antenna 2	Antenna 1	Antenna 2
Flat	1.58	1.45	1.39	1.10	24.09	23.75	22.28	21.17
H-plane	1.96	1.81	1.55	1.32	28.42	27.69	25.83	24.31
E-plane	-0.15	-0.42	-0.71	-1.02	15.14	13.56	12.78	11.02

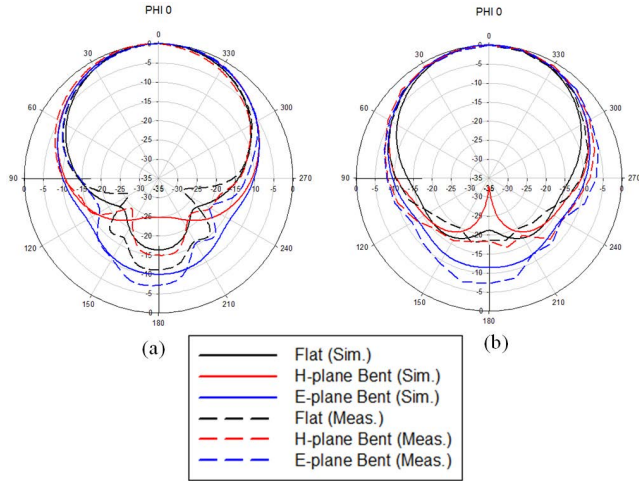


**FIGURE 26.** Radiation pattern of the simulated and measured antenna in flat, H-plane and E-plane bending conditions (a) Antenna 1 (b) Antenna 2.

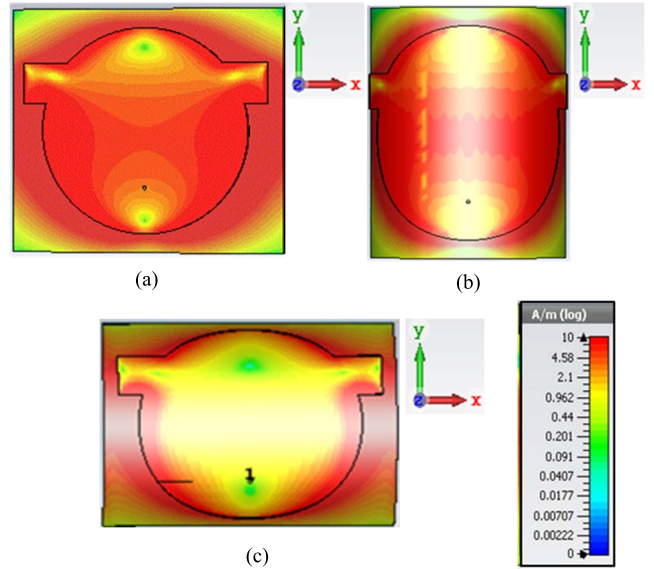


**FIGURE 28.** Current distribution of Antenna 1 (without DGS) in (a) flat, (b) H-plane, and (c) E-plane bending conditions.

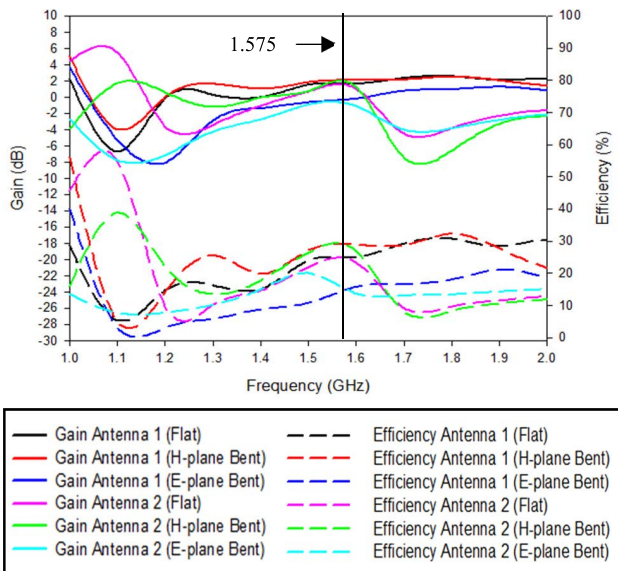


**FIGURE 27.** Graph of gain and efficiency vs frequency for Antenna 1 and 2 in flat, H-plane and E-plane bent condition.

region. The antenna radiating element behaves as a perfect electric conductor at the surface, and hence, the edge. By comparing Antenna 1 and Antenna 2 conditions, the electric field intensity inside the antennas in DGS is around the same values, except for in the centre, where the intensity is slightly higher. Based on theoretical current-voltage

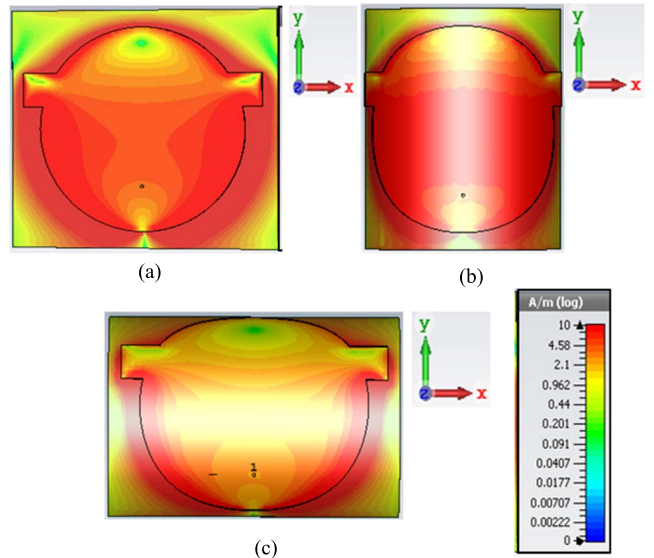


**FIGURE 29.** Current distribution of Antenna 2 (with DGS) (a) flat, (b) H-plane, and (c) E-plane bending conditions.

relation, the observation shows that when a DGS is implemented, more energy is absorbed or radiated to the back of the antenna, which is not preferable, however, this does not significantly reduce the radiated power as the magnitude

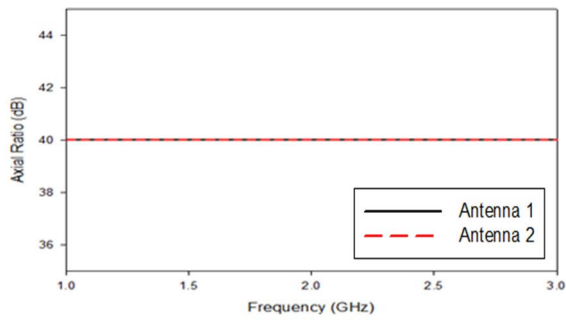


FIGURE 30. Axial ratio of antenna 1 and antenna 2.

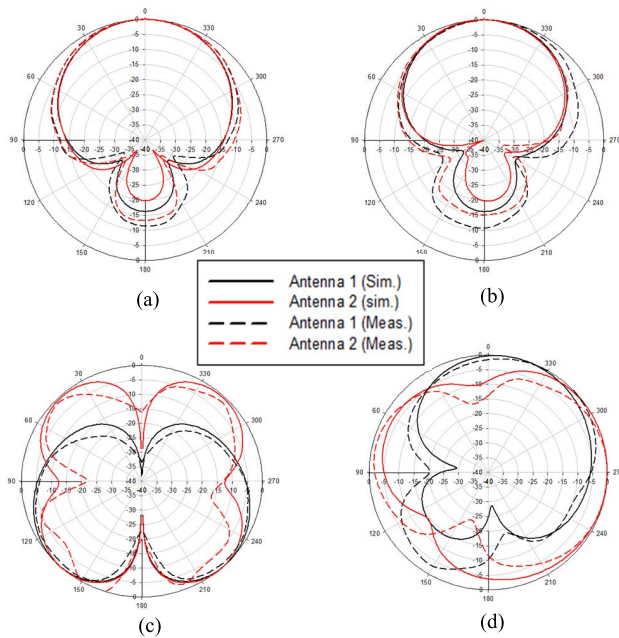


FIGURE 31. Simulated and measured antenna co-polarization at (a) Phi 0 (b) Phi 90 and cross-polarization at (c) Phi 0 (d) Phi 90 in flat condition.

difference remains low. This claim can also be verified based on the simulated antenna gain in Table 3, where it is slightly reduced when DGS slots are added. However, the antenna efficiency does not show significant changes. The difference in efficiency is only 0.34 %, 0.73 %, and 1.78 % for flat, H-plane and E-plane bent respectively.

As shown in Figure 35, the current density on the ground is high at the DGS slot; which is also demonstrated in Figure 36. Based on Figure 36, the magnitude surface currents are almost uniformly distributed throughout the antenna surface, with an average reading of 16.4 A/m and 15.8 A/m for Antenna 1 and 2, respectively. It is crucial to ensure the consistent behaviour of current to validate the correlation between E-field intensity and  $Z_{in}$ . Antenna 2 has a slightly lower magnetic surface current along the radiating edges of the antenna; however, the difference is very small and thus, it does not affect the efficiency significantly. There is a slight deterioration of current distribution in Antenna 2, which is expected due to the presence of DGS slots. When the DGS is implemented at the ground plane, the surface current is still

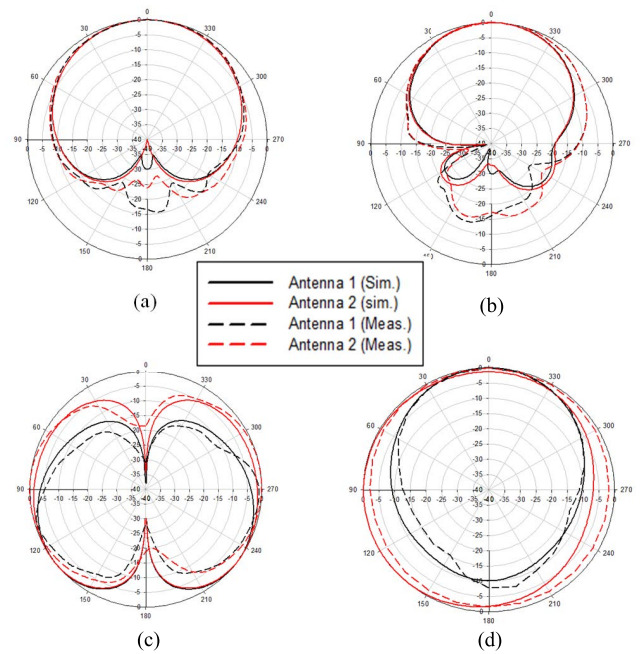


FIGURE 32. Simulated and measured antenna co-polarization at (a) Phi 0 (b) Phi 90 and cross polarization at (c) Phi 0 (d) Phi 90 in H-plane bent condition.

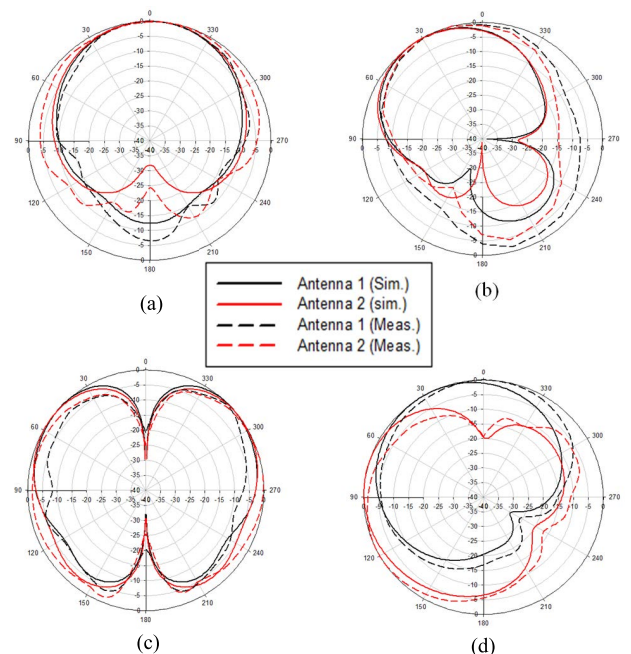


FIGURE 33. Simulated and measured antenna co-polarization at (a) Phi 0 (b) Phi 90 and cross polarization at (c) Phi 0 (d) Phi 90 in E-plane bent condition.

symmetrical; however, it shows a degradation of 6.1 A/m at the exact positions where the vertical slots are located.

There was a back lobe radiation at the specific slot position, which has resulted in the current reduction and, hence, gain degradation. However, the antenna performance is considered acceptable as the gain reduction is not significant, and the design provides more bandwidth to minimize frequency detuning.

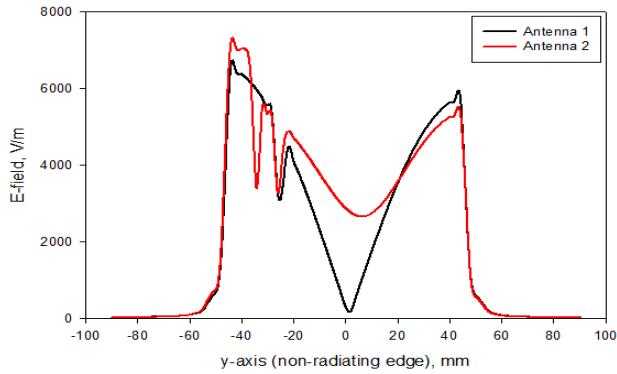


FIGURE 34. Electric field intensity of Antenna 1 and Antenna 2 along the non-radiating edges (y-axis).

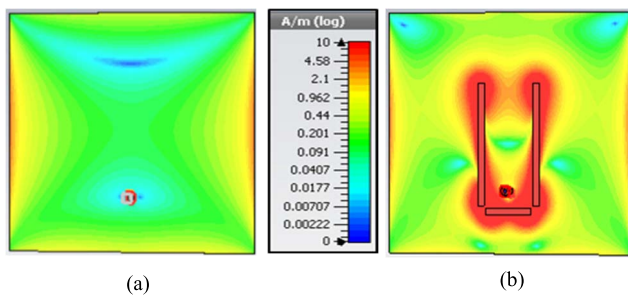


FIGURE 35. Current distribution on the ground of (a) Antenna 1 (without DGS) and (b) Antenna 2 (with DGS).

The comparison of the proposed design with the previous works specifically on bending for GPS applications are shown in Table 4. As compared to the previous work, it is evident that the self-developed electro textile has a comparable performance with the established off-the-shelf materials, considering its gain, efficiency, and antenna size.

From the summarized work in Table 4, researchers in [69], [70] and [71] had studied the effect of bending focussing on H-plane with various bending angles and radius, however, it shows lack of attention is given to the E-plane bent condition. While in [72], the investigation was carried out primarily for E-plane bent conditions with various bending angles. The antenna used which is a truncated rectangular patch was able to alleviate the bending effect on E-plane. However, this experiment was not validated through measurement.

In [73], it is reported that the presence of AMC plane, which was used to increase gain and reduce the antenna back radiation, can alleviate the effects of bending. Yet, the focus on producing a dual-band antenna with dual characteristics has made the antenna design more complex. Based on the previous papers, it is observed that many works have been done to study the deformation effect, such as bending. However the justification through field intensities in E-plane and H-plane configuration was not presented and correlated.

Therefore, in this paper, a textile antenna made of self-developed material with bandwidth enhancement through DGS was designed, simulated, and validated. Although the

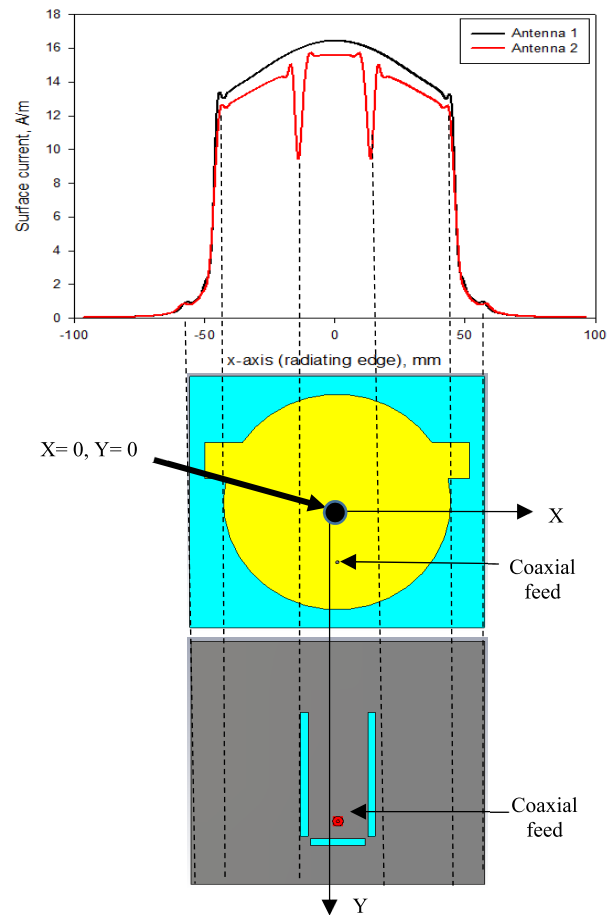


FIGURE 36. Magnetic surface current of Antenna 1 and Antenna 2 along the radiating edges (x-axis).

design method is not new, in this paper, the detailed behaviour of field intensities around the antenna non-radiating and radiating edges have been analyzed to study the effect of DGS. Besides, the proposed antenna has solved the bending issues as the antenna can still operate at the desired frequency during bending along E and H-plane.

**D. EFFECT OF BENDING ON DIFFERENT RADIUS**

In this section, the antenna bending is characterized by the bending radius and was investigated under H and E plane bent conditions as shown in Figure 37. The simulated antenna is bent on a cylindrical foam with  $\epsilon_r$  of 1, and radius R is varied from 42.5 mm to 72.5 mm. The bending effect is studied on both antenna 1 and 2. The simulated results of S-parameters, gain, and radiation pattern are shown in Figure 38, 39, 40, and 41.

From the observation in Figure 38, there is no significant effect on the frequency as the radius varies in both bending conditions for antenna 1. However, there is a slight shift in frequency and  $S_{11}$  of antenna 2, where the bandwidth is also reduced under E-plane bent as the radius increases. Nevertheless, the decrement is acceptable since the antenna still operates at the desired frequency.

TABLE 4. Previous work of textile wearable antenna for GPS application.

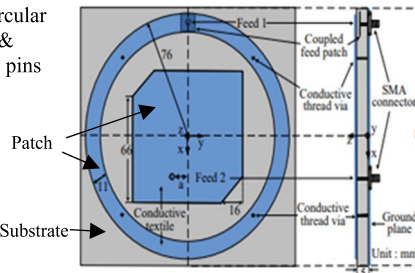
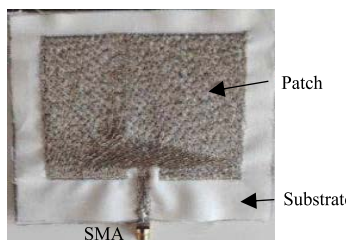
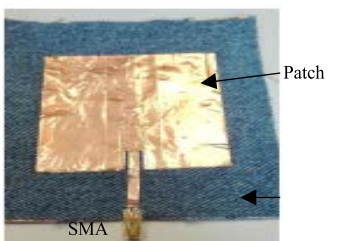
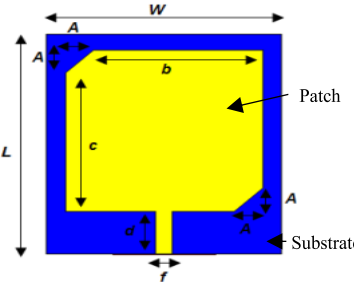
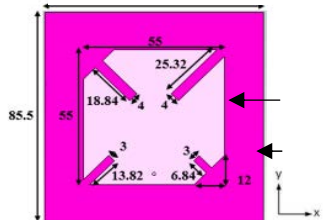
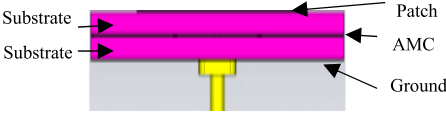
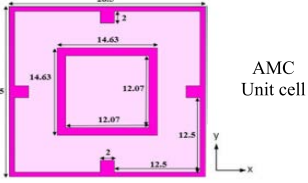
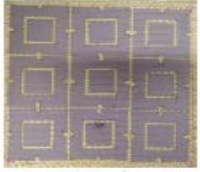
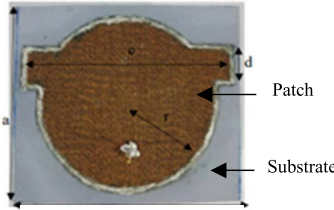
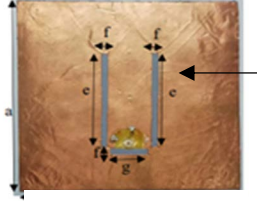
Ref	Parameters	Radiating element & Substrate	Method of design	Design Complexity	Antenna size in term of wavelength (W x L)	Study description
[69]	Frequency (GHz) Bandwidth (GHz) Gain (dB) Efficiency (%)	Shield-It & Felt ( $\epsilon_r = 1.2$ )	Truncated patch, circular ring & shorting pins	Planar textile-based antenna 	$0.83\lambda \times 0.83\lambda$	Deformation effect (Bending on H-plane at bending angle $50^\circ$ and $60^\circ$ ) and SAR on human head
[70]	Frequency (GHz) Bandwidth (GHz) Gain (dB) Efficiency (%)	Silver plated nylon yarn & Cotton ( $\epsilon_r = 1.3$ )	Embroidered antenna, Square patch with insert feed	Planar textile-based antenna 	$0.6\lambda \times 0.6\lambda$	Study of bending (bending on H-plane at human arm) and SAR on human body
[71]	Frequency (GHz) Bandwidth (GHz) Gain (dB) Efficiency (%)	Copper tape & Jeans ( $\epsilon_r = 1.7$ )	Square patch with insert feed	Planar textile-based antenna 	$0.38\lambda \times 0.37\lambda$	Study of bending (bending on H-plane at multiple radius 100 mm, 500 mm and 1000mm) and SAR on human body
[72]	Frequency (GHz) Bandwidth (GHz) Gain (dB) Efficiency (%)	Shield-It, & Felt ( $\epsilon_r = 1.2$ )	Truncated rectangular patch	Planar textile-based antenna 	$0.52\lambda \times 0.59\lambda$	Performance of antenna under bending condition (bending on E-plane at multiple angle, $15^\circ$ , $25^\circ$ , $45^\circ$ , $65^\circ$ , $85^\circ$ )
[73]	Frequency (GHz) Bandwidth (GHz) Gain (dB) Efficiency (%)	Shield-It & Kevlar ( $\epsilon_r = 1.66$ )	AMC (3x3 array of square unit cells with square slit and square ring) truncated patch and slit on patch	Stacked textile-based antenna with AMC array Front View 	$0.45\lambda \times 0.45\lambda$	Parameter study on AMC size and thick, number of arrays and bending effects (Bending on H and E-plane).

TABLE 4. (Continued.) Previous work of textile wearable antenna for GPS application.

					 <p>Side view</p>  <p>AMC Unit cell</p>  <p>AMC Plane</p>		
Proposed antenna	Frequency (GHz)	1.518 – 1.744	Self-developed conductive textile & Polyester ( $\epsilon_r = 1.36$ )	Circular Patch & DGS	Planar textile-based antenna	$0.52\lambda \times 0.47\lambda$	Study the effects of H-plane and E-plane bent condition and mitigates the frequency detuning problem
	Bandwidth (GHz)	0.226			 <p>Front View</p>		
	Gain (dB)	1.45			 <p>Back View</p>		

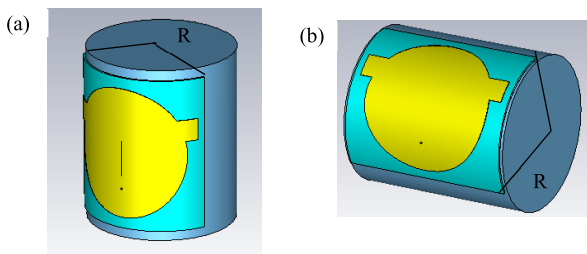


FIGURE 37. Antenna under (a) H-plane and (b) E-plane bent condition with various R.

Bending on different radius also affects the antenna gain and directivity performance. Data in Table 5 shows that the increment in bending radius has increased the antenna gain and directivity. However, the efficiency of the antenna is slightly decreased. The result also agreed with the antenna gain formula in Equation (6). The relationship of antenna

gain,  $G$  is directly proportional to the antenna efficiency,  $\eta$  and directivity,  $D$ , while directivity,  $D$  is inversely proportional to efficiency,  $\eta$ .

$$G = \eta D \approx D = \frac{G}{\eta} \tag{6}$$

In the study, increment in bending radius also indicates decrement in antenna bending angle. The relationship of angle and radius can be described through the arc length,  $S$  formula in Equation (7), where central angle,  $\theta$  is inversely proportional to the circle radius,  $R$ . Therefore, as the radius increases, the bending angle is reduced; hence, the antenna gain increased.

$$S = \theta R \approx \frac{S}{R} = \theta \tag{7}$$

Figure 39 represents the summarized graph for gain and directivity of the antenna. The radiation pattern results in

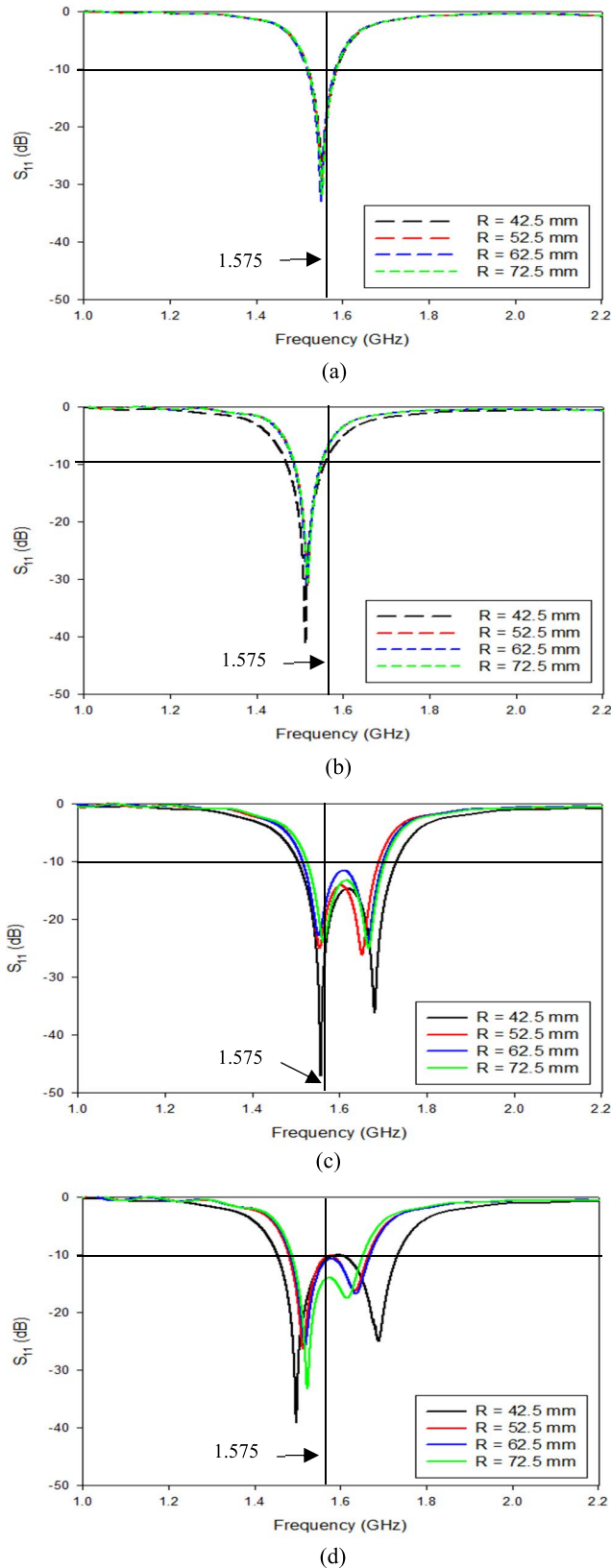


**FIGURE 38.**  $S_{11}$  parameter of antenna 1 at (a) H-plane bent (b) E-plane bent and antenna 2 at (c) H-plane bent (d) E-plane bent under various bending radius.

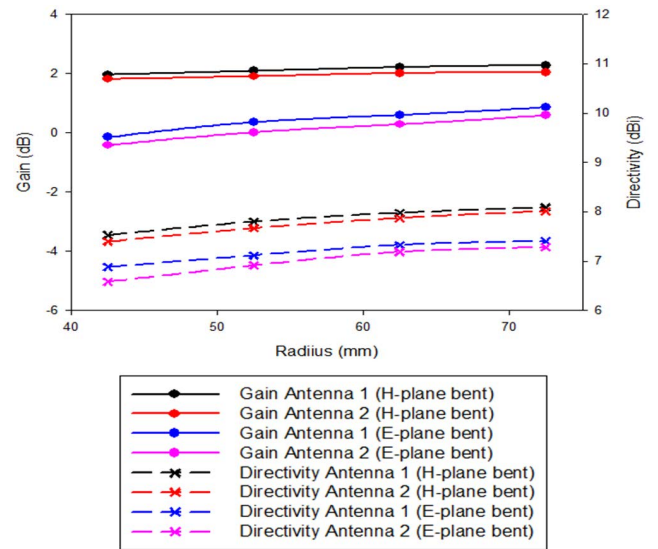


**FIGURE 39.** Gain and directivity of simulated antenna 1 and 2 under various bending radius.

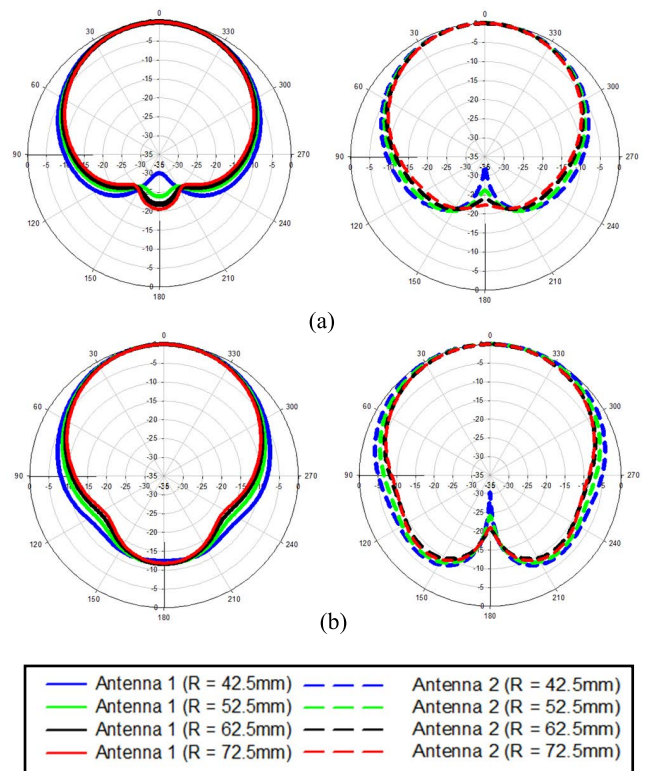


**FIGURE 40.** Radiation pattern of simulated antenna 1 and 2 at (a) H-plane bent (b) E-plane bent under various bending radius.

Figure 40 also agreed with the claim, where it shows a decrement on the side lobe and begins more directive as the radius is increased; thus, the gain is increased. As shown in Figure 41 and 42, this scenario can be clarified with the antenna E-field and H-field intensity.



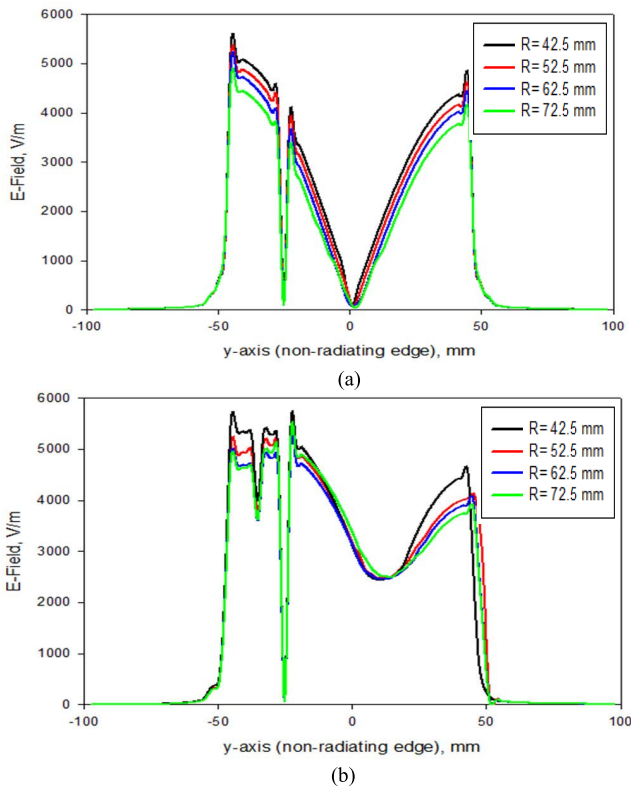


**FIGURE 41.** Electric Field Intensity of (a) Antenna 1 and (b) Antenna 2 along the non-radiating edges (y-axis) under various bending radius.

Since the H-plane bent condition occurs at the y-axis (which is the direction of the electrical field), the electric field (E-field) distribution along the non-radiating edge of the antenna, which is calculated inside the antenna substrate, is observed, as shown in Figure 41. From the graph, the electric field density is zero at the patch surface, showing that the antenna radiating element acts as a perfect electric conductor at the surface. However, approaching the edge of the antenna, E-field increases due to the increment of impedance. Derived based on theoretical current-voltage relation, this E-field observation correlates to impedance increment. Increasing magnitude in E-field indicates more energy is trapped inside the antenna. Therefore, the performance of the antenna will degrade [74].

Based on the graph in Figure 41, both antenna 1 and 2 represent the same trend, where at radius 42.5 mm, the E-field intensity is the highest, and as the radius increased to 72.5 mm, the E-field intensity became lower. This situation indicates that at the highest electric field intensity, more energy is trapped inside the antenna, the impedance is high; thus, the conductivity of the antenna is reduced. As a result, the gain of antenna 1 and 2 is the lowest at radius 42.5 mm, which is 1.96 dB and 1.81 dB, respectively. Meanwhile, at radius of 72.5 mm, which represents the smallest bending angle, less energy is trapped inside the antenna. Therefore, the conductivity of the antenna is high as the impedance is reduced, which then presents the highest gain, 2.28 dB and 2.04 dB for antenna 1 and 2, at 72.5 mm radius.

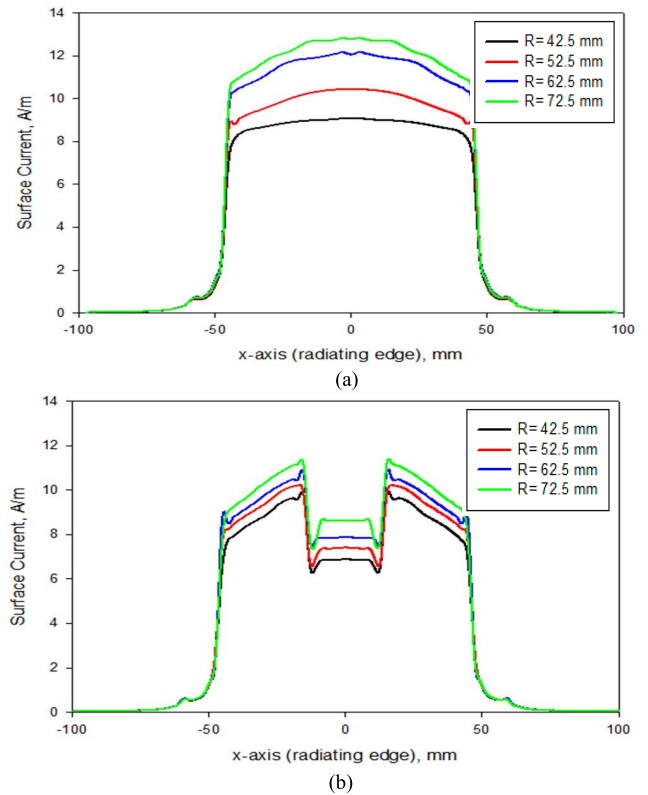


**FIGURE 42.** Magnetic surface current of (a) Antenna 1 and (b) Antenna 2 along the radiating edges (x-axis) under various bending radius.

In Figure 41 (b), the center of the antenna is slightly higher than zero due to the implementation of DGS, where more energy is absorbed and radiated at the back of the antenna.

For antenna under E-plane bent condition, the magnetic field intensity is observed since it occurs at the x-axis (the direction of magnetic field). The magnetic field (H-field) distribution along the radiating edge of the antenna is illustrated in Figure 42. As shown in Figure 42, it is observed that the magnitude current surface is increased as the bending radius increased in both antenna, with an average reading of 9.06 A/m, 10.51 A/m, 12.07 A/m, and 12.89 A/m for antenna 1, and 8.89 A/m, 9.28 A/m, 9.88 A/m and 10.45 A/m for antenna 2, at radius 42.5 mm, 52.5 mm, 62.5mm and 72.5 mm, respectively. The magnitude of the current surface along the radiating edge of the antenna indicates its magnetic field. Therefore, the higher the magnetic surface current, the higher the antenna gain. However, antenna 2 shows a slight degradation at the center of the surface current due to the implementation of DGS.

From the analysis, the effect of bending radius towards the antenna is significant, especially to the antenna gain performance. Study on the antenna E-field and H-field intensity had proven that the antenna with a short radius and big bending angle would reduce the antenna gain performance. This is because more energy is trapped inside the antenna as it is bent on the small bending radius. Hence, the shorter the bending radius, the bigger the bending angle, thus producing lower

**TABLE 5. Simulated antenna 1 and 2 performance under various bending radius at 1.575 GHz.**

	Radius / Central Angle	H-plane Bent				E-plane Bent			
		42.5 mm / 135°	52.5 mm / 109°	62.5 mm / 92°	72.5 mm / 79°	42.5 mm / 135°	52.5 mm / 109°	62.5 mm / 92°	72.5 mm / 79°
Antenna 1	$S_{11}$ (dB)	-13.42	-13.16	-13.36	-13.23	-5.42	-5.59	-5.47	-5.59
	Gain (dB)	1.96	2.08	2.21	2.28	-0.15	0.36	0.60	0.86
	Directivity (dBi)	7.53	7.80	7.98	8.09	6.68	7.12	7.33	7.40
	Efficiency (%)	28.42	27.10	26.78	26.01	15.25	15.49	16.07	16.30
	Bandwidth (GHz)	0.07	0.07	0.07	0.07	0.09	0.06	0.06	0.06
Antenna 2	$S_{11}$ (dB)	-17.70	-17.45	-17.62	-20.08	-11.51	-11.13	-11.67	-14.92
	Gain (dB)	1.81	1.91	2.01	2.04	-0.42	0.02	0.28	0.59
	Directivity (dBi)	7.40	7.66	7.87	8.01	6.58	6.91	7.19	7.28
	Efficiency (%)	27.69	26.51	26.38	25.57	11.41	13.34	13.58	14.38
	Bandwidth (GHz)	0.22	0.18	0.18	0.18	0.28	0.19	0.19	0.17

antenna gain. In addition, the directivity of the antenna is also reduced.

#### IV. CONCLUSION

This study focuses on minimizing the effects of bending on the antenna's operating frequency, where most of the textile-based antennas are known to suffer from frequency detuning under bent conditions. The application of DGS has improved the antenna bandwidth from 4.04% to 12.20%, with the antenna gain of 1.45 dB and radiation efficiency of 23.75%, which has solved the frequency detuning issue. The bending on E-plane is the worst condition since the current deterioration happened at the antenna radiating element; while in H-plane bent condition, the direction of current is in the same direction as the bending condition. Hence the antenna is less affected in H-plane bent condition. At the end of the study, it is proven that by widening the antenna bandwidth, the antenna is able to operate at the desired frequency even under bent conditions. The experiment was successful, and the results have been verified through simulation and measurement.

Based on the electrical field intensity analysis, it is observed that the implementation of DGS had caused more energy to be absorbed or radiated to the back of the antenna, which is not preferable. However, this does not significantly reduce the radiated power as the magnitude difference remains low (only slight degradation in antenna gain is shown). The analysis from the magnetic field intensity also shows that magnetic surface current along the radiating edges of the antenna with DGS is slightly lower than antenna without DGS; however, the difference is very small and thus, does not affect the efficiency significantly. The difference in efficiency for Antenna 1 (without DGS) and Antenna 2 (with DGS) is only 0.34 %, 0.73 %, and 1.78 % for flat, H-plane and E-plane bent, respectively. Meanwhile, the difference in gain for Antenna 1 and 2 is only 0.13dB. The study considers the antenna performance acceptable as the gain reduction is not significant, and the design provides more bandwidth to minimize frequency detuning.

Meanwhile, the effect of bending towards the bending radius does not have a significant impact on the antenna frequency in H-plane bent condition. Only a slight shift in  $S_{11}$ , frequency, and bandwidth is observed on the E-plane bent condition. However, a significant effect could be observed on the antenna gain and directivity performance on both antenna 1 and 2 at H and E-plane bent conditions. The investigation shows that as the radius angle increase, the bending angle decrease. Therefore, the gain and directivity increased. The study is also analyzed its E-field and H-field intensity to prove the concept. From the analysis, as the radius is reduced, the angle of bending increases, more energy is trapped inside the antenna; hence reducing the antenna gain performance and directivity.

From the study, a few considerations and recommendations could be applied in future research to improve antenna's effectiveness in a real application. First is the location of the antenna. The antenna can also be tested on the body area, such as the chest, shoulder, and neck (shirt collar). In this study, the bending radius can be varied depending on its location and the effects can be observed. As for the antenna shape, it is suggested to use a basic symmetrical shape to reduce its impact due to bending. Another crucial parameter that can be studied is the specific absorption rate (SAR) on the human body.

#### ACKNOWLEDGMENT

The authors would also like to thank all researchers of Antenna Research Centre, College of Engineering, Universiti Teknologi MARA, Shah Alam, Selangor, Malaysia, and Textile Research Group, Faculty of Applied Sciences, Universiti Teknologi MARA, for supporting this project.

#### REFERENCES

- [1] M. Alibakhshikenari, B. S. Virdee, L. Azpilicueta, M. Naser-Moghadasi, M. O. Akinsolu, C. H. See, B. Liu, R. A. Abd-Alhameed, F. Falcone, I. Huynen, T. A. Denidni, and E. Limiti, "A comprehensive survey of 'metamaterial transmission-line based antennas: Design, challenges, and applications,'" *IEEE Access*, vol. 8, pp. 144778–144808, 2020, doi: 10.1109/ACCESS.2020.3013698.

- [2] M. Alibakhshikenari, F. Babaecian, B. S. Virdee, S. Aissa, L. Azpilicueta, C. H. See, A. A. Althuwayb, I. Huynen, R. A. Abd-Alhameed, F. Falcone, and E. Limiti, "A comprehensive survey on 'various decoupling mechanisms with focus on metamaterial and metasurface principles applicable to SAR and MIMO antenna systems,'" *IEEE Access*, vol. 8, pp. 192965–193004, 2020, doi: [10.1109/ACCESS.2020.3032826](https://doi.org/10.1109/ACCESS.2020.3032826).
- [3] I. Nadeem, M. Alibakhshikenari, F. Babaecian, A. Althuwayb, B. S. Virdee, L. Azpilicueta, S. Khan, I. Huynen, F. Falcone, T. A. Denidni, and E. Limiti, "A comprehensive survey on 'circular polarized antennas' for existing and emerging wireless communication technologies," *J. Phys. D, Appl. Phys.*, vol. 55, no. 3, p. 33002, Oct. 2021, doi: [10.1088/1361-6463/ac2c36](https://doi.org/10.1088/1361-6463/ac2c36).
- [4] H. Lee, J. Tak, Y. Hong, and J. Choi, "Design of an all-textile antenna integrated in military beret for GPS/RFID applications," in *Proc. Int. Symp. Antennas Propag. (ISAP)*, 2017, pp. 982–983.
- [5] J. Virkki, Z. Wei, A. Liu, L. Ukkonen, and T. Björninen, "Wearable passive E-textile UHF RFID tag based on a slotted patch antenna with sewn ground and microchip interconnections," *Int. J. Antennas Propag.*, vol. 2017, pp. 27–29, Feb. 2017, doi: [10.1155/2017/3476017](https://doi.org/10.1155/2017/3476017).
- [6] M. Niswar, M. Nur, A. A. Ilham, and I. Mappangara, "A low cost wearable medical device for vital signs monitoring in low-resource settings," *Int. J. Electr. Comput. Eng.*, vol. 9, no. 4, pp. 2321–2327, 2019, doi: [10.11591/ijece.v9i4.pp2321-2327](https://doi.org/10.11591/ijece.v9i4.pp2321-2327).
- [7] K. S. Chakradhar, I. V. Rao, D. T. D. Prasad, P. Raju, and V. M. Rao, "Wearable textile patch antenna for medical applications," *Int. J. Innov. Technol. Exploring Eng.*, vol. 9, no. 2S3, pp. 44–47, 2019, doi: [10.35940/ijitee.b1011.1292s319](https://doi.org/10.35940/ijitee.b1011.1292s319).
- [8] O. Vermesan and P. Friess, *Internet of Things: Converging Technologies for Smart Environments and Integrated Ecosystems*. Aalborg, Denmark: River Publishers, 2013.
- [9] B. Xu, "A short review of textile applications in antenna design," *Trends Textile Eng. Fashion Technol.*, vol. 1, no. 5, pp. 119–121, Mar. 2018, doi: [10.31031/tteft.2018.01.000522](https://doi.org/10.31031/tteft.2018.01.000522).
- [10] G. Christina, A. Rajeswari, M. Lavanya, J. Keerthana, K. Ilamathi, and V. Manoranjitha, "Design and development of wearable antennas for tele-medicine applications," in *Proc. Int. Conf. Commun. Signal Process. (ICCCSP)*, Apr. 2016, pp. 2033–2037, doi: [10.1109/ICCCSP.2016.7754532](https://doi.org/10.1109/ICCCSP.2016.7754532).
- [11] A. Kumar, A. Utsav, and R. K. Badhai, "A novel copper-tape wide-band wearable textile antenna for WBAN applications," in *Proc. IEEE Appl. Electromagn. Conf. (AEMC)*, Dec. 2017, pp. 1–2, doi: [10.1109/AEMC.2017.8325660](https://doi.org/10.1109/AEMC.2017.8325660).
- [12] S. B. Roshni, M. P. Jayakrishnan, P. Mohanan, and K. P. Surendran, "Design and fabrication of an E-shaped wearable textile antenna on PVB-coated hydrophobic polyester fabric," *Smart Mater. Struct.*, vol. 26, no. 10, 2017, Art. no. 105011, doi: [10.1088/1361-665X/aa7c40](https://doi.org/10.1088/1361-665X/aa7c40).
- [13] D. Ferreira, P. Pires, R. Rodrigues, and R. F. S. Caldeirinha, "Wearable textile antennas: Examining the effect of bending on their performance," *IEEE Antennas Propag. Mag.*, vol. 59, no. 3, pp. 54–59, Jun. 2017.
- [14] A. Mersani, L. Osman, and J.-M. Ribero, "Effect of bending on the characteristics of a coplanar textile antenna," in *Proc. 18th Medit. Microw. Symp. (MMS)*, Oct. 2018, pp. 255–257.
- [15] N. Amaro, C. Mendes, and P. Pinho, "Bending effects on a textile microstrip antenna," in *Proc. IEEE Int. Symp. Antennas Propag. (APSURSI)*, Jul. 2011, pp. 282–285, doi: [10.1109/APS.2011.5996697](https://doi.org/10.1109/APS.2011.5996697).
- [16] L. Song and Y. Rahmat-Samii, "A systematic investigation of rectangular patch antenna bending effects for wearable applications," *IEEE Trans. Antennas Propag.*, vol. 66, no. 5, pp. 2219–2228, May 2018, doi: [10.1109/TAP.2018.2809469](https://doi.org/10.1109/TAP.2018.2809469).
- [17] P. Salonen and Y. Rahmat-Samii, "Textile antennas: Effects of antenna bending on input matching and impedance bandwidth," *IEEE Aerosp. Electron. Syst. Mag.*, vol. 22, no. 12, pp. 18–22, Dec. 2007, doi: [10.1109/MAES.2007.4408597](https://doi.org/10.1109/MAES.2007.4408597).
- [18] K. N. Paracha, S. K. A. Rahim, P. J. Soh, and M. Khalily, "Wearable antennas: A review of materials, structures, and innovative features for autonomous communication and sensing," *IEEE Access*, vol. 7, pp. 56694–56712, 2019, doi: [10.1109/ACCESS.2019.2909146](https://doi.org/10.1109/ACCESS.2019.2909146).
- [19] M. El Gharbi, M. Martínez-Estrada, R. Fernández-García, S. Ahyoud, and I. Gil, "A novel ultra-wide band wearable antenna under different bending conditions for electronic-textile applications," *J. Text. Inst.*, vol. 112, no. 3, pp. 437–443, 2021, doi: [10.1080/00405000.2020.1762326](https://doi.org/10.1080/00405000.2020.1762326).
- [20] N. P. Gupta, M. Kumar, and R. Maheshwari, "Development and performance analysis of conformal UWB wearable antenna under various bending radii," *IOP Conf. Ser., Mater. Sci. Eng.*, vol. 594, no. 1, 2019, Art. no. 012025, doi: [10.1088/1757-899X/594/1/012025](https://doi.org/10.1088/1757-899X/594/1/012025).
- [21] L. Z. Tung, G. A. Mahdiraji, and L. C. Ping, "Comparative study between planar and bent antenna characterization," in *Proc. MATEC Web Conf.*, vol. 152, 2018, pp. 1–11, doi: [10.1051/mateconf/201815203002](https://doi.org/10.1051/mateconf/201815203002).
- [22] S. N. Mahmood, A. J. Ishak, T. Saeidi, A. C. Soh, A. Jalal, M. A. Imran, and Q. H. Abbasi, "Full ground ultra-wideband wearable textile antenna for breast cancer and wireless body area network applications," *Micromachines*, vol. 12, no. 3, pp. 1–16, 2021, doi: [10.3390/mi12030322](https://doi.org/10.3390/mi12030322).
- [23] M. Tighezza, S. K. A. Rahim, and M. T. Islam, "Flexible wideband antenna for 5G applications," *Microw. Opt. Technol. Lett.*, vol. 60, no. 1, pp. 38–44, Jan. 2018, doi: [10.1002/mop.30906](https://doi.org/10.1002/mop.30906).
- [24] Y. Sun, S. W. Cheung, and T. I. Yuk, "Design of a textile ultra-wideband antenna with stable performance for body-centric wireless communications," *IET Microw., Antennas Propag.*, vol. 8, no. 15, pp. 1363–1375, 2014, doi: [10.1049/iet-map.2013.0658](https://doi.org/10.1049/iet-map.2013.0658).
- [25] M. A. R. Osman, M. K. A. Rahim, N. A. Samsuri, M. K. Elbasheer, and M. E. Ali, "Textile UWB antenna bending and wet performances," *Int. J. Antennas Propag.*, vol. 2012, pp. 1–12, Mar. 2012, doi: [10.1155/2012/251682](https://doi.org/10.1155/2012/251682).
- [26] H. Lago, P. J. Soh, M. F. Jamlos, N. Shohaimi, S. Yan, and G. A. E. Vandenbosch, "Textile antenna integrated with compact AMC and parasitic elements for WLAN/WBAN applications," *Appl. Phys. A, Mater. Sci. Process.*, vol. 122, no. 12, pp. 1–6, Dec. 2016, doi: [10.1007/s00339-016-0575-9](https://doi.org/10.1007/s00339-016-0575-9).
- [27] M. N. Mohanty and V. Gupta, "Design of compact wearable antenna for bandwidth enhancement," in *Proc. Int. Conf. Infocom Technol. Unmanned Syst. (Trends Future Directions) (ICTUS)*, Dec. 2017, pp. 341–345, doi: [10.1109/ICTUS.2017.8286029](https://doi.org/10.1109/ICTUS.2017.8286029).
- [28] P. Jaiswal and P. Sinha, "Design of wearable textile based microstrip patch antenna by using defected ground plane," in *Proc. Int. Conf. Adv. Comput. Telecommun. (ICACAT)*, Dec. 2018, pp. 13647–13651, doi: [10.1109/ICACAT.2018.8933571](https://doi.org/10.1109/ICACAT.2018.8933571).
- [29] N. Gupta, V. K. Singh, Z. Ali, and J. Ahirwar, "Stacked textile antenna for multi band application using foam substrate," *Proc. Comput. Sci.*, vol. 85, pp. 871–877, Jan. 2016, doi: [10.1016/j.procs.2016.05.277](https://doi.org/10.1016/j.procs.2016.05.277).
- [30] M. Li, Q. L. Li, B. Wang, C. F. Zhou, and S. W. Cheung, "A low-profile dual-polarized dipole antenna using wideband AMC reflector," *IEEE Trans. Antennas Propag.*, vol. 66, no. 5, pp. 2610–2615, May 2018, doi: [10.1109/TAP.2018.2806424](https://doi.org/10.1109/TAP.2018.2806424).
- [31] M. Li, R. Wang, H. Yao, and B. Wang, "A low-profile wideband CP end-fire magnetoelectric antenna using dual-mode resonances," *IEEE Trans. Antennas Propag.*, vol. 67, no. 7, pp. 4445–4452, Jul. 2019, doi: [10.1109/TAP.2019.2911399](https://doi.org/10.1109/TAP.2019.2911399).
- [32] A. B. Mustafa and T. Rajendran, "An effective design of wearable antenna with double flexible substrates and defected ground structure for healthcare monitoring system," *J. Med. Syst.*, vol. 43, no. 7, pp. 1–11, 2019, doi: [10.1007/s10916-019-1306-5](https://doi.org/10.1007/s10916-019-1306-5).
- [33] S. Batabyal, S. D. Roy, S. Chakraborty, M. Chakraborty, and A. K. Bhattacharjee, "Wearable DGS integrated high performance compact antenna for 2.45/2.5.8 GHz WLAN band on leather substrate," in *Proc. 2nd Int. Conf. Electron., Mater. Eng. Nano-Technol. (IEMENTech)*, May 2018, pp. 1–8, doi: [10.1109/IEMENTECH.2018.8465336](https://doi.org/10.1109/IEMENTECH.2018.8465336).
- [34] K. Jayabharathy and T. Shanmuganatham, "Design of a compact textile wideband antenna for smart clothing," in *Proc. 2nd Int. Conf. Intell. Comput., Instrum. Control Technol. (ICICT)*, Jul. 2019, pp. 477–481, doi: [10.1109/ICICT46008.2019.8993388](https://doi.org/10.1109/ICICT46008.2019.8993388).
- [35] R. R. Bonaldi, *Electronics Used in High-Performance Apparel—Part 1/2*. Amsterdam, The Netherlands: Elsevier, 2017.
- [36] N. I. Zaidi, M. T. Ali, N. H. A. Rahman, M. S. Amin, A. A. S. A. Shah, and M. F. Yahya, "Comparison of copper covered and copper core sheath yarn for the fabrication of textile antenna," *IIEESR J.*, vol. 13, pp. 1–6, Dec. 2018.
- [37] A. Asghar, M. Ahmad, M. Yahya, M. Ali, A. A. Aziz, N. A. Rahman, S. Z. U. Hassan, and M. Kashif, "An alternative approach to design conductive hybrid cover yarns for efficient electromagnetic shielding fabrics," *J. Ind. Textiles*, vol. 48, no. 1, pp. 38–57, Jul. 2018, doi: [10.1177/1528083717721922](https://doi.org/10.1177/1528083717721922).
- [38] N. I. Zaidi, M. T. Ali, N. H. A. Rahman, M. S. A. Nordin, A. A. S. A. Shah, and M. F. Yahya, "A comprehensive study of weaving structure and its impact on textile antenna for WBAN application," in *Proc. 13th Eur. Conf. Antennas Propag. (EuCAP)*, 2019, pp. 1–5.
- [39] N. H. A. Rahman, Y. Yamada, and M. S. A. Nordin, "Reliability of strip line method for determination of conductivity for lossy conductive materials," *IEEE Access*, vol. 6, pp. 64630–64638, 2018, doi: [10.1109/ACCESS.2018.2877399](https://doi.org/10.1109/ACCESS.2018.2877399).

- [40] N. I. Zaidi, M. T. Ali, N. H. A. Rahman, M. F. Yahya, and M. S. A. Nordin, "Analysis on different shape of textile antenna under bending condition for GPS application," *Bull. Electr. Eng. Informat.*, vol. 9, no. 5, pp. 1964–1970, Oct. 2020, doi: [10.11591/eei.v9i5.2185](https://doi.org/10.11591/eei.v9i5.2185).
- [41] N. I. Zaidi, M. T. Ali, N. H. A. Rahman, M. S. A. Nordin, A. S. A. Shah, M. F. Yahya, and H. Yon, "Analysis of different feeding techniques on textile antenna," in *Proc. Int. Symp. Antennas Propag. (ISAP)*, 2019, pp. 55–57.
- [42] R. C. Mahajan, V. Parashar, V. Vyas, and M. Sutaone, "Design and implementation of defected ground surface with modified co-planar waveguide transmission line," *Social Netw. Appl. Sci.*, vol. 1, no. 3, pp. 1–12, Mar. 2019, doi: [10.1007/s42452-019-0245-6](https://doi.org/10.1007/s42452-019-0245-6).
- [43] M. K. Khandelwal, B. K. Kanaujia, and S. Kumar, "Defected ground structure: Fundamentals, analysis, and applications in modern wireless trends," *Int. J. Antennas Propag.*, vol. 2017, pp. 1–22, Feb. 2017, doi: [10.1155/2017/2018527](https://doi.org/10.1155/2017/2018527).
- [44] A. K. Arya, M. V. Kartikeyan, and A. Patnaik, "Defected ground structure in the perspective of microstrip antennas: A review," *Frequenz*, vol. 64, nos. 5–6, pp. 79–84, Jan. 2010, doi: [10.1515/FREQ.2010.64.5-6.79](https://doi.org/10.1515/FREQ.2010.64.5-6.79).
- [45] N. C. Karmakar, S. M. Roy, and I. Balbin, "Quasi-static modeling of defected ground structure," *IEEE Trans. Microw. Theory Techn.*, vol. 54, no. 5, pp. 2160–2168, May 2006, doi: [10.1109/TMTT.2006.873633](https://doi.org/10.1109/TMTT.2006.873633).
- [46] R. M. Elsagheer, "Study on bandwidth enhancement techniques of microstrip antenna," *J. Electr. Syst. Inf. Technol.*, vol. 3, no. 3, pp. 527–531, Dec. 2016, doi: [10.1016/j.jesit.2015.05.003](https://doi.org/10.1016/j.jesit.2015.05.003).
- [47] S.-J. Guo, L.-S. Wu, and J.-F. Mao, "A wideband microstrip-fed dielectric resonator antenna array with defected ground structure," in *Proc. IEEE Int. Conf. Comput. Electromagn. (ICCEM)*, Mar. 2019, pp. 1–3, doi: [10.1109/COMP.2019.8779170](https://doi.org/10.1109/COMP.2019.8779170).
- [48] P. Patil, S. Goilkar, and N. Deotale, "Microstrip antenna using the defected ground structure for bandwidth enhancement," in *Proc. 4th Int. Conf. Recent Trends Electron., Inf., Commun. Technol. (RTEICT)*, May 2019, pp. 1384–1388, doi: [10.1109/RTEICT46194.2019.9016853](https://doi.org/10.1109/RTEICT46194.2019.9016853).
- [49] M. Challal, M. Dehmas, A. Azrar, R. Aksas, and M. Trabelsi, "Circuit modeling and EM simulation verification of DGS based low-pass filter employing transmission line model along with microstrip-slotline transitions," in *Proc. MATEC Web Conf.*, vol. 52, 2016, pp. 1–6, doi: [10.1051/mateconf/20165201003](https://doi.org/10.1051/mateconf/20165201003).
- [50] A. K. Arya, M. V. Kartikeyan, and A. Patnaik, "Defected ground structure in the perspective of microstrip antennas: A review," *Frequenz*, vol. 64, nos. 5–6, pp. 79–84, Jan. 2010, doi: [10.1515/FREQ.2010.64.5-6.79](https://doi.org/10.1515/FREQ.2010.64.5-6.79).
- [51] A. I. R. Garg, P. Bhartia, and I. J. Bahl, *Microstrip Antenna Design Handbook*. Norwood, MA, USA: Artech House, 2001.
- [52] P. kumar Deb, T. Moyra, and P. Bhowmik, "Return loss and bandwidth enhancement of microstrip antenna using defected ground structure (DGS)," in *Proc. 2nd Int. Conf. Signal Process. Integr. Netw. (SPIN)*, Feb. 2015, pp. 25–29, doi: [10.1109/SPIN.2015.7095318](https://doi.org/10.1109/SPIN.2015.7095318).
- [53] V. Vaid and S. Agrawal, "Bandwidth optimization using fractal geometry on rectangular microstrip patch antenna with DGS for wireless applications," in *Proc. Int. Conf. Med. Imag., m-Health Emerg. Commun. Syst. (MedCom)*, Nov. 2014, pp. 162–167, doi: [10.1109/MedCom.2014.7005996](https://doi.org/10.1109/MedCom.2014.7005996).
- [54] D. Fistum, D. Mali, and M. Ismail, "Bandwidth enhancement of rectangular microstrip patch antenna using defected ground structure," *Indonesian J. Electr. Eng. Comput. Sci.*, vol. 3, no. 2, pp. 428–434, 2016, doi: [10.11591/ijeecs.v3.i2.pp428-434](https://doi.org/10.11591/ijeecs.v3.i2.pp428-434).
- [55] L. H. Weng, Y.-C. Guo, X.-W. Shi, and X.-Q. Chen, "An overview on defected ground structure," *Prog. Electromagn. Res. B*, vol. 7, pp. 173–189, 2008, doi: [10.2528/pierb08031401](https://doi.org/10.2528/pierb08031401).
- [56] D.-J. Woo, T.-K. Lee, J.-W. Lee, C.-S. Pyo, and W.-K. Choi, "Novel U-slot and V-slot DGSs for bandstop filter with improved Q factor," *IEEE Trans. Microw. Theory Techn.*, vol. 54, no. 6, pp. 2840–2847, Jun. 2006.
- [57] D.-J. Woo, T.-K. Lee, C.-S. Pyo, and W.-K. Choi, "High-Q band rejection filter by using U-slot DGS," in *Proc. Eur. Microw. Conf.*, 2005, pp. 1279–1282.
- [58] T. R. Kuphaldt, *Alternating Current AC* (Design Science Licence), vol. 2, 6th ed. Chapel Hill, NC, USA: Univ. of North Carolina Press, 2007.
- [59] M. D. Elton, "Analyzation of the resistor-inductor-capacitor circuit," *Undergraduate J. Math. Model., One + Two*, vol. 7, no. 2, pp. 1–19, 2017, Art. no. 1, doi: [10.5038/2326-3652.7.2.4876](https://doi.org/10.5038/2326-3652.7.2.4876).
- [60] M. Capek, L. Jelínek, and P. Hazdra, "On the functional relation between quality factor and fractional bandwidth," *IEEE Trans. Antennas Propag.*, vol. 63, no. 6, pp. 2787–2790, Jun. 2015, doi: [10.1109/TAP.2015.2414472](https://doi.org/10.1109/TAP.2015.2414472).
- [61] H. R. Sanjari, A. A. Merati, S. M. H. Varkiyani, and A. Tavakoli, "Evaluation of the effect of bending on the resonance frequency of inset-fed rectangular textile patch antenna," *J. Ind. Textiles*, vol. 46, no. 1, pp. 19–44, 2016, doi: [10.1177/1528083715569377](https://doi.org/10.1177/1528083715569377).
- [62] S. Yan and G. A. E. Vandenbosch, "Radiation pattern-reconfigurable wearable antenna based on metamaterial structure," *IEEE Antennas Wireless Propag. Lett.*, vol. 15, pp. 1715–1718, 2016, doi: [10.1109/LAWP.2016.2528299](https://doi.org/10.1109/LAWP.2016.2528299).
- [63] Y. Mukai, V. T. Bharambe, J. J. Adams, and M. Suh, "Effect of bending and padding on the electromagnetic performance of a laser-cut fabric patch antenna," *Textile Res. J.*, vol. 89, no. 14, pp. 2789–2801, Jul. 2019, doi: [10.1177/0040517518801202](https://doi.org/10.1177/0040517518801202).
- [64] (2020). *Series Resonance Circuit*. [Online]. Available: <https://www.electronics-140.tutorials.ws/accircuits/series-resonance.html>
- [65] A. M. D. Thanu, M. Devadoss, and K. Parasuraman, "Analysis of voltage and current magnification in resonant circuits on hyperspectral signal processing," *Meas. Control*, vol. 53, nos. 3–4, pp. 635–648, Mar. 2020, doi: [10.1177/0020294019877495](https://doi.org/10.1177/0020294019877495).
- [66] M. Rizwan, L. Sydänheimo, and L. Ukkonen, "Impact of bending on the performance of circularly polarized wearable antenna," *Prog. Electromagn. Res. Symp.*, vol. 2015, pp. 732–737, 2015.
- [67] S. Chakraborty, R. Poddar, S. Chattopadhyay, and R. Guha, "Wide beam microstrip patches with grounded E-shaped edges to improve the polarization purity," in *Proc. 3rd Int. Conf. Found. Frontiers Comput. Commun. Electr. Eng. (CE)*, 2016, pp. 75–78.
- [68] A. Ghosh and B. Basu, "Rectangular microstrip antenna with defected patch surface for miniaturization and improved polarization purity," in *Advances in Computer, Communication and Control*, vol. 41. Singapore: Springer, 2019, doi: [10.1007/978-981-13-3122-0](https://doi.org/10.1007/978-981-13-3122-0).
- [69] H. Lee, J. Tak, and J. Choi, "Wearable antenna integrated into military berets for indoor/outdoor positioning system," *IEEE Antennas Wireless Propag. Lett.*, vol. 16, pp. 1919–1922, 2017, doi: [10.1109/LAWP.2017.2688400](https://doi.org/10.1109/LAWP.2017.2688400).
- [70] I. Gil and R. Fernández-García, "Wearable embroidered GPS textile antenna," in *Proc. Prog. Electromagn. Res. Symp.-Spring (PIERS)*, May 2017, pp. 655–659.
- [71] I. Gil and R. Fernández-García, "Wearable GPS patch antenna on jeans fabric," in *Proc. Prog. Electromagn. Res. Symp. (PIERS)*, Aug. 2016, pp. 2019–2022.
- [72] M. S. Shakhirul, M. Jusoh, A. H. Ismail, M. I. Jais, M. R. Kamarudin, and M. N. Osman, "Analysis of circular polarization textile antenna in bending condition," in *Proc. Int. Conf. Comput., Commun., Control Technol. (I4CT)*, Apr. 2015, pp. 360–363.
- [73] R. Joshi, E. F. N. M. Hussin, P. J. Soh, M. F. Jamlos, H. Lago, A. A. Al-Hadi, and S. K. Podilchak, "Dual-band, dual-sense textile antenna with AMC backing for localization using GPS and WBAN/WLAN," *IEEE Access*, vol. 8, pp. 89468–89478, 2020, doi: [10.1109/ACCESS.2020.2993371](https://doi.org/10.1109/ACCESS.2020.2993371).
- [74] N. H. A. Rahman, Y. Yamada, and M. S. A. Nordin, "Analysis on the effects of the human body on the performance of electro-textile antennas for wearable monitoring and tracking application," *Materials*, vol. 12, no. 10, pp. 1–17, 2019, doi: [10.3390/ma12101636](https://doi.org/10.3390/ma12101636).



**NORSYAHIRAH IZZATI ZAIDI** was born in Negeri Sembilan, Malaysia. She received the B.Eng. degree in electrical engineering (electronic) from the Universiti Malaysia Pahang, Pekan, Malaysia, in 2015, and the M.Sc. degree in telecommunication and information engineering from the Universiti Teknologi MARA (UiTM), Shah Alam, Malaysia, in 2017, where she is currently pursuing the Ph.D. degree in electrical engineering. She has experience in working as an Assistant Lecturer. Her research interests include textile antenna, flexible antenna, weaving pattern analysis, and electromagnetic analysis for wearable application. She has published a number of journal articles and conference papers and has won gold medals in several local and international competitions, such as FKE-IIID 2017, International Conference and Exposition in Invention of Institution of Higher Learning (PECIPTA 2017), and Virtual Invention Innovation & Design FKE 2020 (VIID FKE 2020). She is a Graduate Engineer of the Board of Engineering Malaysia (BEM).



**NURUL HUDA ABD RAHMAN** (Member, IEEE) received the M.Eng. degree in electronic from the University of Surrey, Guildford, U.K., in 2008, and the Ph.D. degree in electric, electronic and systems engineering from the Universiti Kebangsaan Malaysia, in 2014. She joined Astronautic Technology (M) Sdn. Bhd., as a Spacecraft Engineer, in 2008, where she was involved in various small-class satellite development and research and development projects. In 2014, she was appointed as a Senior Lecturer with the Universiti Teknologi MARA Malaysia (UiTM). She is currently working with UiTM. She also received a 2-year Postdoctoral Fellowship under the Malaysia-Japan International Institute of Technology, Universiti Teknologi Malaysia, from 2018 to 2019. Her current research interests include antennas for space and terrestrial applications, array antennas, reflector and lens antennas, wearable and flexible antennas, RF and microwave design, and electromagnetic analysis. She has been the Professional Engineer of the Board of Engineers Malaysia (BEM), since 2019. She has been appointed as the Executive Committee of the IEEE Malaysia AP/MTT/EMC Joint Chapter during 2021–2022. She was a recipient of the Best Professional Paper Award IEEE Malaysia Comsoc & VTS Joint Chapter in 2018 and the Best Paper Award from IEEE Malaysia AP/MTT/EMC Joint Chapter in 2018 and 2019.



**MOHAMAD FAIZUL YAHYA** has been at the Textile Technology Program, Faculty of Applied Sciences, Universiti Teknologi MARA, Shah Alam, since 2003. At the moment, he is developing weave CAD model and material properties of multitude numerical analysis procedures for modeling tensile and impact behavior of woven fabric. He published 40 scientific articles in high impact journals, book, magazines, and conference proceedings. He is also very active in supervising nine postgraduate research (Ph.D. and M.Sc.) students, mostly in 2D/3D woven fabric research topics. His main research interests include geometrical modeling and finite element analysis simulation of 2D/3D woven fabrics dry and composites. He won one diamond (special award), four gold, six silvers, and six bronze medals in research product competition, both locally and overseas. Until today, he had given ten invited academic lecturers requested by government and industries. Most of his lectures were in the Woven Fabric Technology field.



**MUHAMMAD SHAKIR AMIN NORDIN** was born in Shah Alam, Selangor, Malaysia. He received the B.Eng. degree in electronic communication engineering from the Universiti Teknologi MARA, Shah Alam, in 2016, where he is currently pursuing the M.Sc. degree in electrical engineering in the area of electro-textile antenna for GPS tracking application. He has experience in working as an Assistant Lecturer. He is also a Researcher at the Antenna Research Center, Universiti Teknologi MARA. He has published a number of journal articles and conference papers. His research interests include wearable antenna design and electromagnetic radiation analysis. He has won gold medals in several local and international competitions, such as FKE-IID 2017, International Conference and Exposition in Invention of Institution of Higher Learning (PECIPTA 2017), and Virtual Invention Innovation & Design FKE 2020 (VIID FKE 2020).



**SUHAILA SUBAHIR** received the B.Eng. and M.Sc. degrees in electrical engineering from the Universiti Teknologi Malaysia (UTM), Johor, Malaysia, in 1999 and 2002, respectively, and the Ph.D. degree in electrical engineering from the Universiti Teknologi MARA. She is currently a Senior Lecturer at the Universiti Teknologi MARA (UiTM), Selangor, Malaysia. Her research interests include communication antenna design, integrated antenna, RF devices and circuits, and electromagnetic radiation analysis. She also as an Active Member of Professional Engineer, Board of Engineers Malaysia, The Institution of Engineers, Malaysia (IEM), and the IEEE RFID Chapter. She has been awarded the Innovative Dedicated Research Professional by Innovative Scientific Research Professional Malaysia (October 2017). She was elected as a Treasurer of the IEEE AP/MTT/EMC Joint Chapter (2005–2010), then was elected as a Treasurer of the IEEE Malaysia Section (2013–2015).



**YOSHIHIDE YAMADA** received the bachelor's and master's degrees in engineering from the Nagoya Institute of Technology, in 1971 and 1973, respectively, and the Ph.D. degree in electrical engineering from the Tokyo Institute of Technology, in 1989. He joined Electrical Communication Laboratories, Nippon Telegraph and Telephone Corporation (NTT), in 1973, and moved to NTT Mobile Communications Network, Inc., (NTT DoCoMo), in 1993. In 1998, he joined National Defense Academy, as a Professor. In 2014, he joined the Malaysia Japan International Institute of Technology, Universiti Teknologi MARA (UTM), Malaysia, as a Professor. His research interests include aperture antennas, array antennas, very small antennas, and radar cross sections. He is a fellow of the IEICE Japan, a Senior Member of IEEE APS, and a member of ACES. He received the Excellent Paper Award and the Best Tutorial Paper Award from IEICE in 2013 and 2014, respectively.



**ABHIJIT MAJUMDAR** graduated (Hons.) from the Textile Technology Program, Calcutta University, in 1995. He received the M.Tech. degree in textile engineering from the IIT Delhi, the Ph.D. degree in production and operations management from Jadavpur University, Kolkata, and the M.B.A. degree from the IIT Delhi with specialization in Operations Management. He joined the Department, as an Assistant Professor, in 2007. He is currently a Professor with the Department of Textile & Fibre Engineering, Indian Institute of Technology, Delhi. He worked in industries, such as Voltas Ltd., and Vardhman Group. He has published 75 research articles in international refereed journals and guided six Ph.D. students. He has authored a textbook entitled *Principles of Woven Fabric Manufacturing* (CRC Press). He has also edited two books published by Woodhead Publisher, U.K., and authored one monograph (Textile Progress) published by Taylor and Francis. He is an Associate Editor of *Journal of the Institution of Engineers (India) Series E (Chemical and Textile Engineering)* (Springer). His research interests include protective textile materials, soft computing applications, and operations and supply chain management. He was a recipient of the Outstanding Young Faculty Fellowship (2009–2014) of the IIT Delhi, the Teaching Excellence Award (2015) of the IIT Delhi, and the Gandhian Young Technological Innovation Award (2017).

...